# FEASIBILITY OF SMALL VOXEL SIZES IN CANINE BRAIN $^{1}$H-MAGNETIC RESONANCE SPECTROSCOPY AT 3T

By

DAINNA KRISTINE STELMACH

(Under the Direction of Simon R. Platt & Shannon P. Holmes)

## ABSTRACT

Initial studies in proton magnetic resonance spectroscopy ($^{1}$H-MRS) of the canine brain have used large voxel sizes, resulting in non-specific spectra. Multi-voxel chemical shift imaging (CSI) $^{1}$H-MRS was performed on eight neurologically normal research dogs using a GE 3.0T Signa HDx MR unit with a single-channel knee coil. MRSI $^{1}$H-MRS was performed in the thalamus (Thal), piriform (Pirif) lobe and cerebellar medulla (CereMed). The following voxel sizes were assessed: 0.5, 0.4, 0.3 and 0.225 cm$^{3}$. Descriptive statistics were performed on major metabolites (Cho, NAA, Cr) and metabolic ratios. Major metabolite means, ratios and % baseline noise were compared for significance across each voxel size. The scans were performed within a clinically applicable time, and of acceptable quality, with moderate baseline noise. We determined that smaller voxel sizes can be achieved for $^{1}$H-MRI of the canine brain, resulting in minimal voxel contamination, particularly when using a 0.225 cm$^{3}$ voxel.

INDEX WORDS: $^{1}$H-MRS, MR spectroscopy, Canine, Brain, Voxel, Normal

# FEASIBILITY OF SMALL VOXEL SIZES IN CANINE BRAIN $^{1}$H-MAGNETIC RESONANCE SPECTROSCOPY AT 3T

By

DAINNA K. STELMACH

B.A., The University of Colorado at Boulder, 2002

D.V.M., Western University of Health Sciences, 2009

This Thesis Submitted to the Graduate Faculty of The University of Georgia in Partial Fulfillment of the Requirements for the Degree

MASTERS OF SCIENCE

ATHENS, GEORGIA

2014

# FEASIBILITY OF SMALL VOXEL SIZES IN CANINE BRAIN $^{1}$H-MAGNETIC RESONANCE SPECTROSCOPY AT 3T

by

DAINNA KRISTINE STELMACH

Major Professors: Simon Platt
Shannon Holmes

Committee: Mark Kent
David Jiménez

Electronic Version Approved:

Julie Coffield
Interim Dean of the Graduate School
University of Georgia
August 2014

TABLE OF CONTENTS

Page

LIST OF TABLES

Page

LIST OF FIGURES

Page

# Title: INTRODUCTION

Nuclear magnetic resonance (NMR) spectroscopy has been used as an analytical technique in chemistry to determine the structure of compounds and composition of mixtures of compounds. This technique is also commonly applied to *in vitro* and *in vivo* research as well as in a clinical setting and was renamed magnetic resonance spectroscopy (MRS) so to avoid the negative connotations associated with the term "nuclear."[1,2] *In vivo* this technique allows the examination of the biochemical status of living tissue in a non-invasive manner.[3] Most MRS research and clinical applications of magnetic resonance spectroscopy have involved the human brain. Examples include MRS of human brain tumors and brain abscesses, which typically require invasive surgical or ultrasound-guided biopsies for definitive diagnoses. Research over the past few decades has elucidated that the use of MRS in these disease processes may aid in diagnoses and monitoring treatment, without the use of invasive techniques. MRS in animals has typically been in the context of models for human neurologic diseases. Recently, the clinical utility of MRS in veterinary medicine has become a topic of discussion.

## THE PHYSICS OF MRS

### MR ACTIVE NUCLEI

Atoms with an odd mass number (i.e. number of protons and neutrons are not the same) have innate nuclear net spin (angular momentum) in one direction. Nuclei possessing angular momentum that can be detected using MR techniques are known as MR active nuclei.[4-7] The laws of electromagnetic induction involve three forces- motion, magnetism and charge. These laws state that if two of these forces are present, then the third will automatically be induced. For example, the hydrogen proton ($^{1}H$) is the most commonly examined MR active nucleus in both MR imaging (MRI) and MRS. Hydrogen contains one positively charged proton with an innate spin (i.e. motion) and therefore, a magnetic field is induced around the atom. Hydrogen MRS is often referred to as proton MRS or $^{1}H$-MRS. On account of the electrical charge that MR active nuclei posses, they will align their axis of rotation when placed in an applied external magnetic field. Most nuclei will align in the same direction as the applied magnetic field (in parallel or spin-up), while a slightly smaller proportion will align in the opposite direction of the field (anti-parallel or spin-down). The spin-down state is a higher energy state than the spin-up state.[4-7] While in these orientations, each nucleus is innately spinning on its axis.

A second effect of an external magnetic field is to induce the spinning nucleus to wobble around the applied magnetic field, similar to a spinning top. This induced wobble is called precession.[4,6,7] The frequency of precession, called

the Larmor frequency, is fundamental to all MR techniques. This Larmor frequency is dependent on magnetic field strength (B) and the gyro-magnetic ratio (g). The gyromagetic ratio is a different value for each MR active nucleus (e.g. $^{13}C$, $^{1}H$, $^{31}P$). When different MR active nuclei are placed in the same magnetic field strength, each will precess at different, unique frequencies. The gyromagnetic ratio of a hydrogen nucleus is 4.1 x $10^7$ Hz/Tesla. Therefore, the Larmor frequency of Hydrogen in a 1.0-Tesla (T) magnetic field is 42.58 MHz. Using specific Larmor frequencies allows the selective detection of specific MR active nuclei (e.g. $^{1}H$), while ignoring the signals from other MR active nuclei in the body.[4] Knowing the specific Larmor frequency of an MR active nucleus is important because it allows selective excitation of that nucleus. MR techniques use applied radiofrequency (RF) pulses at the exact Larmor frequency of the nucleus, referred to as the resonance frequency, to cause specific nuclear excitation. After receiving the resonance frequency RF pulse, the MR active nucleus will temporarily reach a higher energy status. When the applied RF pulse is terminated, the MR active nucleus will return to its equilibrium state and will emit a specific, detectable nuclear signal. These signals are emitted at very specific, differing frequencies for different types of molecules containing MR active nuclei (e.g. $^{1}H$ in water). Within a molecule, the MR active nuclei are exposed to slightly different magnetic fields due to local environmental differences. This creates what is called a chemical shift in the frequency. It is these slightly different frequencies for each different molecule that results in

distinctive signature peaks in the MR spectrum. These peaks are signal intensity representations of molecular concentrations.[3 7,8]

The hydrogen nucleus is the most commonly utilized MR active nucleus in conventional MRI and MRS. $^{1}H$ is the ideal nucleus for MR techniques because of its high gyromagnetic ratio, high natural abundance, and a favorable relaxation time (time to return to equilibrium after excitation).[1,2] These factors contribute to hydrogen producing the largest detectable signal of all of the MR active nuclei, per nuclear component. In contrast, other MR active nuclei, such as $^{13}C$, $^{15}N$ and $^{31}P$ have lower sensitivity (due to smaller gyromagnetic ratios) and lower natural abundance. Detection of these other nuclei requires specialized equipment, such as RF coils adjusted to the resonance frequency of these nuclei. In MRS research these nuclei are used to study certain diseases, such as $^{31}P$ in the study of muscle, due to the presence of phosphorus in ATP. Evaluation typically requires using higher magnetic field strengths and longer scan times to compensate for a smaller signal created by these nuclei.[1,9] Other factors including temperature have an impact on the signal produced.[1] MR signal is calculated with the following equation,

$$S \propto M_o\omega_o = NB_o^2\gamma^3\hbar^2 I(I+1)/3kT$$

S is the signal detected in the receiver coil, Mo is the magnetization, $\omega_o$ is the resonance frequency, N is the total number of spins in the sample, $B_o$ is the main magnetic field strength, $\gamma$ is the gyromagnetic ratio of the selected nuclei, I is the spin quantum number, k is the Boltzmann constant ($1.380650 \times 10^{-23}$ $JK^{-1}$), T is

the absolute temperature in Kelvin (K), and $\hbar$ = h (Planck's constant) /2∏. Based on this equation, the highest signal is obtained at high magnetic field strengths, using nuclei with a high gyromagnetic ratio (i.e. hydrogen) and at a low temperature (in Kelvin, which has minimal influence in biologic tissues).[1]

Although MRS uses the same MR active nucleus, equipment, and similar techniques (to be discussed later) as conventional MRI, MRS produces a spectrum. In contrast, MRI produces a 2-dimensional image representation of MR spectra within a volume of tissue.[2,4] In order for a compound to be detectable using MRS, the compound must be a small, mobile or flexible molecule, and in concentrations of 0.5-10 millimols (mM) within the extracellular or cellular spaces.[2] For the most part, large or membrane bound molecules exhibit broad resonances that contribute to the baseline spectrum and are therefore undetected.[1] Changes in local tissue chemistry are detected as changes in the MRS peaks of particular molecules, and provide information on metabolic pathway changes. MRS is therefore an appropriate technique for the non-invasive monitoring of disease and response to treatments.[2]

$^{1}$H-MRS has been used to evaluate multiple body systems in humans, including the prostate, breast tissue and brain. The brain has been the most extensively studied due in part to the relative difficulty of definitive diagnoses using more invasive techniques, such as tissue biopsy. $^{1}$H-MRS can analyze numerous neuro-metabolites in the brain in order to diagnose and monitor certain diseases. These neuro-metabolite molecules include choline (Cho), creatine (Cr),

N-acetyl aspartate (NAA), glutamine (Glu), glutamate (Gln), GABA, myoinositol (mI) and certain amino acids. Alterations in these molecules may be detected with MRS in the absence of observable gross alterations in tissue morphology and signal intensity in conventional MR images. [2,5,10 11] For this reason, $^{1}$H-MRS has proven to be important in human studies of stroke, neoplasia, multiple sclerosis and neurodegenerative diseases.[1] Well-established spectroscopic profiles for these and other disease states in humans has allowed improved prognostication, earlier treatment due to earlier diagnoses, and better assessment of response to treatment or progression of disease.[11]

**HOW MRS IS ACQUIRED**

MRS requires a strong, static external magnetic field, a radiofrequency coil that will produce and also sometimes receive signals, and gradient coils (Gx, Gy and Gz) used to produce separate magnetic fields in the x-, y- and z-planes respectively. These are the same components used in MRI units, which is why many will have MRS capabilities. The gradient fields are used to selectively excite a small volume of interest (VOI) in the tissue. This is necessary to acquire a detectable signal that is used to produce a spectrum exclusively from a specifically selected area.[1,2,4,6,7,9] Clinical MRS requires the acquisition of a conventional MRI imaging series to provide anatomic information and facilitate the placement of the MRS VOI within a specific tissue region.[12]

## CHOICE OF ECHO TIME

Similar to conventional MRI, changing the echo time (TE) changes the information that is obtained. The metabolites that can be identified using MRS are in part due to the TE. Short TEs offer the advantage of decreased signal decay, which allows visualization and quantification of metabolites with short relaxation times, such as lipids, along with metabolites that show up at longer TEs.[13,14] Using clinical magnetic field strengths, most metabolites can be identified using an intermediate to long TE of 144-288 ms. These include NAA, Cho, Cr, and sometimes lactate. Longer TEs are used more commonly for MRS because these techniques are less susceptible to artifacts from insufficient water suppression and have a flatter baseline, making analysis simpler.[15] Using protocols with shorter TEs (< 40ms), additional metabolite peaks, such as Glu, Gln and mI can be identified.[16] Additionally, a characteristic doublet peak of lipid may be seen at 1.2 ppm when using shorter TEs. Lipids may be difficult to differentiate from or obscure the resonance peak of lactate. However, when an intermediate TE (135-144ms) is used, lactate can be identified by its characteristic inverted peak at 1.31 ppm. The identification of lipid and lactate is of particular importance, because they are absent from normal brain tissue, with exception of lipid contamination from outside of the brain. Lipids may indicate the presence of necrosis due to fatty acid breakdown products of cell membranes.[1,13,17,18] The differentiation of these is equally important because lactate is a marker of anaerobic metabolism and has been associated with

infarcts, neoplasia and multiple sclerosis.[1] It was determined that the presence of lipid and lactate in neuroepithelial tumors had a strong correlation with the World Health Organization (WHO) grade.[18] Also, lipid signals have been shown to be more readily detectable in high and intermediate grade gliomas using short TE techniques (30 ms) when compared to intermediate TE techniques (136 ms).[19]

## SINGLE VOXEL AND MULTI-VOXEL MRS

There are two main methods for acquiring MRS. The VOI can be placed in a single discrete region of tissue, know as single-voxel MRS (SVMRS) or from a larger region that is divided into multiple voxels, known as magnetic resonance spectroscopic imaging (MRSI) or chemical shift imaging (CSI). Two and three-dimensional techniques are available for both methods.[1,2,4 16]

### SINGLE VOXEL TECHNIQUES

The two most commonly used acquisition sequences for single voxel spectroscopy include STEAM (Stimulated Echo Acquisition Mode) and PRESS (Point Resolved Spectroscopy Sequence).[1,4,20] In the STEAM sequence, three 90-degree refocusing pulses are used to collect the signal. This sequence allows shorter echo times and a sharper slice profile, but this is at the expense of signal-to-noise ratio (SNR) by approximately a factor of 2. PRESS uses 180-degree refocusing pulses as the second and third RF pulses and is less sensitive to motion than STEAM.[1,2,4,20] SVMRS is designed so that signals outside of the

selected voxel volume are eliminated, usually using slice selection pulses with good excitation profiles, shimming, crusher gradients and outer volume suppression pulses.[1,21]

## MULTI-VOXEL TECHNIQUES

For MRSI, a volume of interest is selected using STEAM or PRESS and then phase encoding gradients are applied in 2 or 3 dimensions (2D or 3D). Spectra of all voxels are acquired simultaneously and then subdivided into smaller voxels. One of the biggest disadvantages of CSI, compared to SVMRS, is out of voxel magnetization and voxel bleed. Ideally, the slice selective pulse would create a perfect slice profile, and all tissue outside of that slice would be dephased by strong crusher gradients. In reality there will always be a small amount of residual magnetization from outside of the desired voxel.[1] This is due in part to truncation artifacts caused by limited k-space sampling, which is commonly employed in MRSI to decreased scan time. This allows signal from outside of the nominal voxel to contribute to the voxel's spectrum.[1] This is a significant issue associated with magnetic resonance spectroscopic imaging (MRSI) where a large volume of tissue is divided into multiple smaller voxels, each giving rise to a spectrum simultaneously.[2] In MRSI the magnetic field homogeneity must be optimized over a large volume of tissue, which can be challenging. With MRSI, any variations in the magnetic field can broaden the signal so that closely spaced peaks are difficult to resolve, and water is

suppressed incompletely in some voxels and over-suppressed in others.[12] One of the advantages of MRSI is that there is greater brain coverage, allowing analysis of larger regions at a time and comparing one area of the brain to another. MRSI techniques are more time consuming and can be challenging to fit the volume of interest into certain anatomic regions because of the rectangular shape.[1] In general, MRSI is used to obtain information on spatial distributions.[2]

## CHEMICAL SHIFT

In brain MRS, the compounds of primary interest, such as NAA and Cho, have MR active hydrogen protons within their molecular structure. The precise frequency emitted by these metabolites depends on the molecular environment surrounding hydrogen protons and interactions with neighboring molecules. For example, the response of NAA to a radiofrequency pulse differs from the response of water by approximately 178 Hz because the methyl group of NAA is partially shielded from the magnetic field by an electron cloud. Water has an oxygen atom that draws electrons away from the hydrogen nuclei, leaving them exposed to the magnetic field. The small difference in resonance frequencies, called chemical shift, is usually enough to differentiate between the two on an MRS spectra. However, the spectra plotted on the x-axis are not labeled in Hertz (Hz), but instead in parts per million (ppm) for convenience and consistency between magnetic field strengths. The numerical value for each metabolite in ppm for each metabolite will be the same at each magnetic field strength

because the separation in Hz is proportional to field strength.[5,22] Most signals of interest are located in a spectral region covering only hundreds of Hz, or 4-5 ppm. If the signal from two molecules is too close in proximity, it can be difficult to resolve them as separate molecules. This problem is less significant at higher magnetic frequencies. For instance, glutamate (Glu) and glutamine (Gln) have significant overlap at 1.5 T and are therefore commonly referred to as the combined signal from these molecules (Glx). Glu and Gln are more easily differentiated from one another at 2.0T and even more so at 4.0T.[5]

**MAGNETIC FIELD STRENGTH**

High field magnet systems result in improved signal to noise ratio, and are therefore ideal for performing MRS. With higher field strengths, however, come some limitations. With SVMRS, the chemical-shift frequency spread increases linearly with field strength, which would decrease the accuracy of the voxel spectra.[23] To overcome this, the bandwidth of the RF pulses must increase in proportion with the field strength, thus minimizing chemical shift. Increasing the bandwidth necessitates shortening the RF pulse length, which requires the use of increased RF power. Fortunately, despite increases in RF power deposition, $^{1}$H-MRS techniques can usually be performed without exceeding safe levels of RF power deposition in humans.[23] The proton spectrum produced by brain tissue is made up of a series of metabolic signatures (i.e. peaks) that cumulatively create

an overlapping complex of peaks, forming a spectrum. The appearance of which will vary with magnetic field strength.[11]

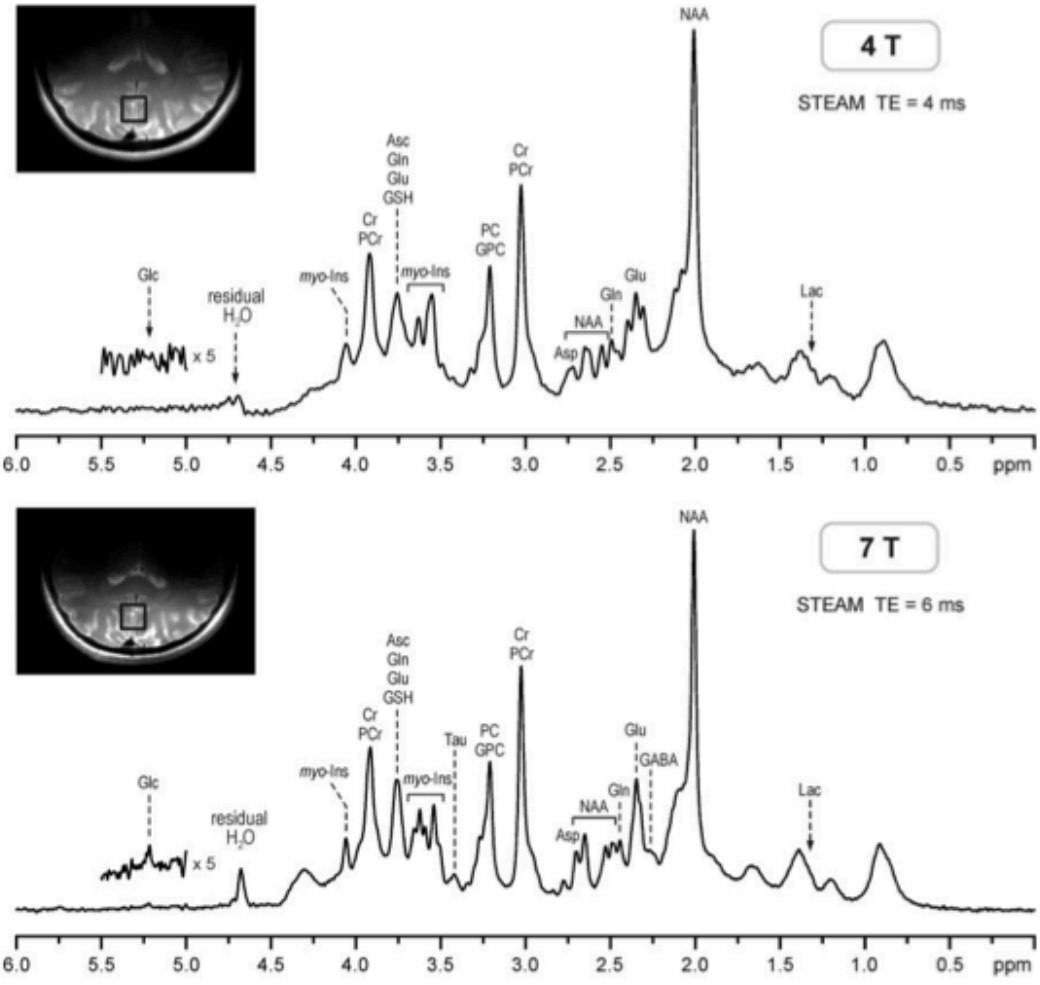


**Figure 1.** *In vivo*, human brain $^{1}$H– SVMRS at 4.0 and 7.0 Tesla field strengths. At these high field strengths, seventeen brain metabolites were identified. At 7.0T, there is increased quantification and detection of weakly represented metabolites, when compared to 4.0T. [24] Tkac *et. al.* 2009

## WATER AND FAT SUPPRESSION

With $^{1}$H-MRS, there is also the issue of interference by the prominent signals from lipids and water. The signal from water in the brain is in the 100,000 mM range, while most brain metabolites are in the 1-30 mM range.[2] For this reason, many techniques are utilized to suppress the signals from fat and water, which makes resolution of smaller metabolite signals possible.[5] Water suppression can be achieved by pre-saturating the water signal using 90-degree pulses or during the localization sequence through selective 180-degree pulses and crusher gradients.[1] Lipid suppression may also be achieved by avoiding excitation of lipid-containing regions. This can be achieved by means of localization, via pre-saturation techniques, or using inversion pulse selection to exploit the difference in T1 values between lipids and other molecules. Another technique involves frequency selective saturation pulses, but this would also exclude the signals from compounds that resonate at a similar frequency, such as lactate or alanine.[1]

## POST ACQUISITION DATA ANALYSIS

The goal of $^{1}$H-MRS analysis is to determine the relative concentrations and concentration ratios of the molecules in the spectra. Two basic methods can be used to analyze the magnetic resonance spectra: time domain processing and frequency domain processing. Time domain MRS can be referred to as a measurement domain, because it is a true representation of raw data. The

amplitude of the time-domain signal is directly proportional to the number of molecules producing the signal. The decay constant of the signal is determined by the mobility and precession frequency of the molecules. This combined information will characterize the identity of a molecule.[12]. Using the frequency domain function analysis renders data to be interpretable to the human eye. In order to convert the data from the time domain to the frequency domain, a Fourier transform (FT) must be performed.[1,12] Quantifying MRS signals in the time domain or frequency domain are also achieved using complex mathematical model functions that will not be discussed in detail. If the measured signal has adequate signal to noise ratio (SNR), without truncation artifacts or baseline distortion, then the time domain and frequency domain functions will obtain similar results, with regard to calculation of molecular concentrations. Essentially, the signal voltage created in the receiver coil by a molecule is directly proportional to the concentration of the molecule detected in an area of interest.[1,12] Any signal interference will create differences in the molecular concentrations measured using the two different methods.[12] Additionally, distortion of the spectrum may occur, which creates a rolling baseline. Immobile molecules with short relaxation times will contribute to spectra with broad bandwidths. A baseline originating from macromolecules makes baseline approximation more difficult.[12] Baseline correction techniques may be applied to address for this. Time-domain calculations may require more computational time and memory, when compared to the frequency domain. In general, time domain

methods do not rely on equally spaced sampling intervals, which may be more useful for multidimensional MRSI.[12]

## BRAIN METABOLITES DETECTED WITH $^{1}$H - MRS

### N-ACETYL-ASPARTATE (NAA)

In Health:

In brain $^{1}$H-MRS, the most prominent peak in the proton spectrum is N-acetyl-aspartate (NAA). Its resonance peak at 2.01 ppm mostly originates from the methyl group of N-acetyl aspartate. Some of the signal contribution comes from N-acetylaspartyl glutamate (NAAG) at 2.04 ppm, but this is resolved only using high field strengths.[1,2] NAA is synthesized in the neurons of the normal brain, travels along axons and is broken down within the oligodendrocytes.[25,26] NAA is also found within oligodendrocyte type 2 astrocyte progenitor cells and immature oligodendrocytes.[16] In humans, NAA levels are low in the developing brain, despite the presence of neurons and axons. NAA levels gradually increase in the fetal brain in utero and in the neonatal brain.[25] This same increase in NAA with neonatal brain development has been documented in rats studied at postnatal days 7, 10, 14, 21 and 28.[27] In the neonatal rat brain, it was noted that NAA levels were normally lower in the striatum, compared with the hippocampus and cerebral cortex between days 14 and 28 in the postnatal period.[27]

NAA molecules are formed from glucose (Glc) metabolism.[28] NAA is released into extracellular fluid (ECF), where it diffuses to oligodendrocytes.

Oligodendrocytes are the only source of the catabolic enzyme, amidohydrolase II, where NAA is deacetylated to form aspartate (Asp). Asp is recycled in large part back to neurons via an active transport mechanism.[28]

NAA performs several functions in the central nervous system (CNS), one important role of NAA appears to be osmoregulatory, in which the NAA cycle operates as a molecular water pump (MWP) in the brain between neurons and oligodendrocytes.[26] Human brain produces and must remove metabolic water at approximately 12 times the rate of the rest of the body. This MWP is of utmost importance because neurons lack water channels such as aquaporins.[26]

In Disease:

Since NAA is produced in the neuron and uses axonal transport as part of the normal metabolism, any disease that is associated with neuronal and/or axonal loss will cause a decrease in NAA on the $^{1}$H-MRS spectra.[25,29] In humans, extra-axial tumors such as meningiomas can have significantly decreased levels of NAA or lack the peak completely because of their non-neuronal origin.[16,17,30] The concentration of NAA is significantly decreased for several days after ischemic brain injury, but eventually increases back to near normal levels.[25,31] A decrease in brain NAA is demonstrated through $^{1}$H-MRS after radiation therapy in brain tissue adjacent to an irradiated tumor that appears normal with conventional MRI.[32] In a study of Simian immunodeficiency virus, it was noted that NAA was significantly decreased in the frontal cortex when peak viremia was

achieved after infection. This was suggestive of regionally specific neuronal damage, and an increase to near normal NAA levels after plasma viral loads decreased significantly, indicating that NAA changes may be reversible in some diseases.[33] In humans with Canavan's leukodystrophy, there is a relative increase in NAA noted. Canavan's disease is an autosomal recessive hereditary leukodystrophy resulting from deficiency of the enzyme aspartoacylase. The deficiency of aspartoacylase leads to increased concentration of NAA in brain and body fluids.[34,35] This is the only disease process that has shown to result in an increase in NAA in humans.[16]

Research has indicated that evaluation of NAA through $^{1}$H-MRS may be important for the early identification of ischemic brain insult, as has been demonstrated in a canine stroke model.[31] A study involving changes in the $^{1}$H-MRS in dogs, as a model for human ischemic brain insult noted that NAA levels significantly decreased 3 days after ischemic insult and increased 10 days after insult. It is thought that the residual signal of NAA may be from surrounding normal brain rather than from the infarct itself. [31]

CREATINE (Cr)

In Health:

The Creatine (Cr) methyl group creates a significant peak in the $^{1}$H-MRS spectra at 3.0 ppm. A smaller peak from the methylene group ($CH_2$) of creatine can sometimes be found at 3.91 ppm.[1,36] The Cr peak in the $^{1}$H-MRS spectrum represents both creatine and phosphocreatine (PCr) in approximately equal amounts in normal brain tissue. The two metabolites are in a constant equilibrium to replenish ATP levels as needed.[25]

Cr is synthesized predominantly within the liver and transported to the brain.[1] However, L-arginine:glycine amidinotransferase (AGAT) and guanidinoacetate methylltransferase (GAMT), the two enzymes of the creatine synthesis pathway, are well expressed within CNS, suggestive of autonomous brain Cr synthesis.[37] Absence of one of these enzymes or the specific Cr transporter, SLC6A8, in the brain will result in early clinical signs of neurologic dysfunction to varying degrees in young children.[37] Similar to NAA, Cr concentrations are low in newborn humans compared with the $^{1}$H-MRS spectra of adults.[25] In neonatal rats, thought to be good models for human neonatal brain development, there is a 2-fold increase in Cr between postnatal days 7 and 28.[27] Cr has also been shown to increase in the parietal region of normal aging humans.[38]

When $^{1}$H-MRS was performed on cell cultures of 90-95% purity, Cr was most significantly concentrated within oligodendrocytes compared with other cell

types. Cr was found in the lowest concentrations in meningeal cells and neurons.[36] In the normal human brain, Cr concentrations are significantly higher in cerebellum compared to parieto-occipital gray matter, occipital white matter and pons. This is thought to reflect the high energy demand of cerebellar Purkinje cells and lack of Cr within the dense axonal and neuronal tissue of the pons.[39]

In Disease:

Brain Cr concentrations are considered to be stable, even in diseased states. Thus, many metabolite concentrations are reported as ratios, using creatine as the denominator.[40] However, it has been shown in a research setting that Cr concentrations can vary significantly.[41] In certain disease states, such as pyogenic brain abscesses, Cr, a marker of normal energy metabolism, will be absent from $^{1}$H-MRS spectra.[29] In large, acute, demyelinating lesions, such as in multiple sclerosis (MS), transient decreases in Cr can be seen.[42] It has been noted that in relapsing MS patients, in brain regions greater than 1.5 cm from visible MS plaques, there is a significant increase in the white matter Cr compared with gray matter Cr.[43] Due to the fact that Cr concentrations are significantly higher in glial cells compared with other cell types [36], an increase in Cr in perilesional tissue without changes in NAA or Cho may be correlated with reactive gliosis without inflammation. This has been confirmed histologically in white matter that appears normal on conventional MRI.[43,44] Studies performed in rats and humans have also found a significant decrease in Cr and PCr in areas of

acute ischemic stroke or infarct.[45,46] Because of the changes in Cr demonstrated with $^{1}$H-MRS of numerous disease states, some have argued that it is more accurate to report metabolite concentrations as absolute quantities as opposed to their ratios with other metabolites such as Cr.[16,41]

MYO-INOSITOL (mI)

In Health:

Myo-Inositol (mI) is a sugar-like substance found in the brain that resonates at 3.6 ppm and can be visualized on the $^{1}$H-MRS spectra when a pulse sequence is acquired using a short TE.[25] Myo-inositol is thought to be important in astrocyte osmoregulation under hypertonic conditions. Its uptake in the cell in this environment is mediated by a $Na^{+}$ -dependent co-transporter.[47]

Myo-inositol is synthesized in glial cells and is absent in neurons; it has therefore been used as a glial cell marker. The highest levels of mI were noted in the hippocampus when compared with the cerebral cortex and striatum in normal developing neonatal rat brains. [27]

In Disease:

Myo-Inositol concentrations may fluctuate significantly with different metabolic states and diseases.[11] An increase has been noted with glial proliferation or with increase in glial cell size such as gliosis and in Alzheimer's disease in humans.[16] A significant increase in mI with or without an increase in

Cho in conjunction with a decrease or complete lack of NAA has been strongly associated with histologically diagnosed primary brain tumors in children and adults.[48] This is seen because of the obliteration and replacement of normal brain tissue with proliferating abnormal neoplastic cells such as anaplastic astrocytes in glioblastomas.[49] Gliosis is differentiated from a glial cell tumor by only mild decreases in NAA and moderate increases in mI and Cho. However, cases of severe gliosis can mimic the $^{1}$H-MRS spectra of brain tumors. [48] A progressive and stable increase in mI is noted in all brain regions after infection with Simian immunodeficiency virus in macaques and has been similarly elevated in studies with HIV patients.[33]

CHOLINE (Cho)

In Health:

Choline (Cho) is another prominent peak on the $^{1}$H-MRS spectra located at 3.2 ppm. The peak is formed from the combined resonances of several Cho-containing metabolites. These compounds are involved in phosphatidylcholine synthesis and breakdown. Phosphatidylcholine accounts for approximately 60% of the total phospholipids found in eukaryotic cells.[25]

Both Cho and mI are high in the newborn human brain, but rapidly decrease in the first one to two years of human life.[25,50] Similarly, phosphorylcholine and glycerophosphorylcholine levels decrease significantly in neonatal rats between postnatal days 7 and 28.[27] This same study, when

focusing on regional variation in metabolites, determined that the highest Cho levels can be found in the striatum when compared to the hippocampus and cerebral cortex in normal developing neonatal rat brain.[27]

The large Cho peak noted early in life, as compared with the adult brain, is thought to be associated with the high demand for substrates needed for the formation of myelin and cell membranes. The active process of myelination in the human brain, including oligodendrocyte differentiation and proliferation, lipid deposition and myelin sheath formation, occur most dramatically between mid-gestation and before 2 years of age.

The decreased choline peak noted in association with human brain development may be associated with a relative completion of myelination and the corresponding incorporation of phosphatidylcholine into the mature myelin sheaths.[25] A meta-analysis of 18 studies comparing young to older brain $^{1}$H-MRS spectra in humans noted a significant increase in Cho in the parietal region in normal aging patients.[38]

In Disease:

Similar to Myo-Inositol (mI), Choline (Cho) levels have been shown to change in response to alterations in membrane metabolism or when membranes are damaged. Because choline is a normal constituent of cell membranes, pathologic processes such as pyogenic brain abscesses may cause a complete absence of Cho on $^{1}$H-MRS.[29]

Cho levels on $^{1}$H-MRS can become significantly decreased in normal appearing brain tissue on MRI that has received therapeutic doses of irradiation for an adjacent brain tumor.[32] Examination of Cho through $^{1}$H-MRS has been suggested as a non-invasive measurement of early neurologic dysfunction in otherwise normal appearing brain tissue during and after radiation treatments.[32]

Increases in Cho have also been shown to be associated with pathologic processes involving glial proliferation (especially oligodendrocytes). When seen in conjunction with decreases in NAA, it is associated with histologically diagnosed brain tumors in humans.[48] The elevated Cho seen in brain tumors is thought to be associated with cellular hyperplasia, neuronal degeneration and myelin degradation.[51] In vitro $^{1}$H-MRS studies have shown an increased Cho is due to the increased levels of phosphocholine (PCho) specifically.[52,53]

GLUTAMATE (Glu) and GLUTAMINE (Gln)

In Health:

Glutamate (Glu) and glutamine (Gln) are indistinguishable at 1.5 T and lower magnetic field strengths due to a significant spectral overlap between their resonances. As a result they can be identified as a complex of peaks, designated the acronym (Glx), at 2.05 and 2.5 ppm. The use of higher field strength magnets, however, provides the ability to quantify these metabolites seperately.[16,54] Another complicating factor is that the Glx complex has a short T2 relaxation value of 80-100ms at 1.5 T. However, in routine brain studies a TE of

approximately 144 ms is commonly used. One study involving tumefactive demyelinating lesions used a phantom model to compare Glx on $^{1}$H-MRS with Glx at normal physiologic concentrations (10 mmol, 20 mmol and 50 mmol).[55] Glx was not discernible at 10 mmol with a TE of 144 ms, but when increased to 20 and 50 mmols, peaks were noted at 2.01-2.5 ppm and 3.65-3.8 ppm, respectively.[55]

Both Glu and Gln are essential for neurotransmission, but Glu is stored mostly in neurons while Gln is found in astrocytes.[25] In neonatal rat brain development, there was a significantly greater amount of Glu noted in the normal cerebral cortex compared with the hippocampus and stratum on postnatal days 14, 21 and 28.[27] It has been documented that Glu and Gln gradually increase in the normal developing rat brain between postnatal days 7 and 28.[27] Changes in Glu and Gln concentrations have been noted with normal aging. A study by Kaiser *et al.* examined the age-related changes in Glu and Gln in the normal aging human brain at 4.0 T. In their study, there was a significantly lower concentration of Glu noted predominantly in the gray matter motor cortex of older patients compared with the younger group. They also noted a trend of increasing Gln predominantly in the white matter of the corona radiata in the older group of patients.[54] It was thought that the Glu reduction in gray matter associated with age might indicate decreased neuronal metabolism or possible neuronal loss or shrinkage with aging. This was supported by a finding of reduced NAA, a putative neuronal marker, in the gray matter of aged patients in the same study.[54] The

increased concentration of Gln in the white matter of older patients could indicate glial cell proliferation in white matter with normal aging. Interestingly, in support of this theory, increased Gln occurred with concurrent increases in mI, a glial cell marker.[54]

In Disease:

Glu, acting on receptors such as N-methyl-D-aspartate (NMDA), is thought to play an important role in cell death subsequent to seizures, cerebral ischemia, and traumatic brain injury.[56] Excessive synaptic Glu may cause nerve cell damage because of excessive excitation.[25] In patients with hepatic encephalopathy, there is an increase formation of Gln from Glu in the presence of ammonia.[10,57] Significantly elevated cerebral Gln levels have been detected using $^{1}$H-MRS in patients with chronic hepatic encephalopathy compared with normal controls and in people with liver disease without encephalopathy.[57]

The cerebral Glx levels have been shown to be elevated after traumatic brain injury in adults and children.[58] In adult humans with acute traumatic brain injury, Glx elevation in occipital gray and parietal white matter was associated with significantly worse outcomes.[59] In patients with epilepsy, elevated levels of glutamate have been measured in the cerebrospinal fluid (CSF) and increased detectable glutamate was found in biopsy samples taken from human epileptic cortex. It has been postulated that the evaluation of Glu with GABA using $^{1}$H-MRS may help define an area of epileptic focus in humans.[60] Evaluation of brain

Glx concentrations may also be useful in the diagnosis of neoplasia. Glial cell tumors have been shown to release Glu, which causes excitotoxic death to surrounding neurons, thereby vacating room for tumor expansion.[61] In one study using $^{1}$H-MRS to differentiate types of glial cell tumors, the specific feature of oligodendrogliomas was the presence of the Glx peak.[62]

GAMMA - AMINOBUTYRIC ACID (GABA)

In Health:

Gamma-Aminobutyric acid (GABA) is the major inhibitory neurotransmitter in the mammalian brain. The human brain contains a concentration of approximately 1 mM of GABA. The chemical structure of GABA consists of three different methylene groups. The signals of these methylene groups are overlapped by larger resonances of Cr (3.03 ppm), Glx (2.3 ppm) and NAA (2.01 ppm).[63,64] At magnetic field strengths below 3.0 T, differentiation between GABA and these more prevalent compounds is difficult. There are three ways in which signal overlap is reduced: spectral editing techniques, spreading signal out in two-dimensional $^{1}$H-MRS and increased magnetic field strength.[64]

In Disease:

A study using a 7.0 T magnet showed GABA and Glu tissue concentration to be significantly decreased in the fronto-parietal cortex and hippocampus of rats under ischemic conditions.[60] In humans, disease conditions involving GABA

studied with $^{1}$H-MRS include epilepsy, motor disorders, mood and anxiety disorders, schizophrenia, alcoholism and drug addition, sleep disorders, migraines, autism, and olfactory and gustatory disorders.[65]

Epilepsy, anxiety disorders and sleep disorders are clinically applicable in veterinary medicine as well. Animal models of epilepsy have indicated that GABA is decreased in seizure states. Cortical biopsies from human epilepsy patients have not shown consistent changes in GABA, however, which is likely because GABA levels continue to increase during ischemia associated with surgical resection of tissue.[66]

LACTATE (Lac)

In Health:

Lactate (Lac) is another important metabolite studied via $^{1}$H-MRS. The Lac molecule has two, weak resonances, a doublet at 1.33 ppm due to methyl protons and a quartet at 4.1 ppm due to the methine proton.[67] In healthy tissue under normal conditions, Lac levels are too low to be detectable, even using high magnetic field strengths.[16] A small Lac signal is sometimes observed within the ventricular cerebrospinal fluid. This is thought to be due to either higher concentrations of Lac when compared to brain parenchyma, or due to a longer T2 relaxation time.[1,68]

Lac is often difficult to distinguish from overlapping lipid resonance peaks, especially when there is voxel contamination from adjacent adipose tissue within

the scalp. The simplest method for distinguishing lactate from lipid is to use a TE of approximately 140 ms, resulting in the Lac to be out of phase, causing the peak to be inverted.[1,67]

In Disease:

Lactate is an oxidation and reduction (REDOX) partner of pyruvate. Under conditions of adenosine triphosphate (ATP) utilization, when oxygen availability is low, the rate of anaerobic glycolysis may exceed oxidative metabolism. The tricarboxylic acid (TCA) cycle rate decreases causing pyruvate to be converted to lactate. Lac therefore potentially functions as a marker for a range of pathologic conditions.[67,69]

Lac can be detected when levels become elevated in association with certain disorders, such as pyogenic brain abscesses and in the developing brain, in which pyruvate dehydrogenase has decreased activity.[16,25,29] The concentration of Lac in brain tissue increases with ischemia, due to the presence of anaerobic metabolism and may reflect neuronal damage.[16,31,60] In neonates with hypoxic-ischemic injury, there is elevated detectable brain Lac within the first 24 hours of injury.[25] There are detectable levels in tissue regions with poor washout (cysts, necrotic tissue and hydrocephalus).[16] Some studies indicate that Lac is present in the brains of healthy elderly people and senescent rats and may therefore be a possible marker for aging.[60]

## LIPIDS

### In Health:

Lipids have short relaxation times and are only visualized with a short TE under normal conditions. They produce large, broad peaks at 0.8 and 1.5 ppm.[16] The concentration of free lipids is extremely small in normal tissue.

### In Disease:

In certain pathologic states involving cell membrane breakdown and release of fatty acids, lipid peaks will become detectible with $^{1}$H-MRS.[25] The presence of lipid may indicate voxel contamination by adipose tissue when placed near structures such as the scalp or subcutaneous tissue.[1,16]

## AMINO ACIDS

### In Health:

Amino acids are less commonly detected compounds in normal brain, and are difficult to detect because they are very small and/or have spectroscopic peaks that overlap with other substances.[1] For example, the amino acid taurine is an osmolite that is synthesized from cysteine by astrocytes and not primary neurons.[70] A study on normal neonatal rat brain development revealed a significant decrease in taurine between neonatal days 7 and 28.[27]

In Disease:

The presence of amino acids (valine, isoleucine and leucine) on $^{1}$H-MRS can be a sensitive marker of pyogenic brain abscesses, but their absence cannot rule it out.[29] Abscesses contain large amounts neutrophils and protein. Proteolytic enzymes are released with the breakdown of neutrophils, which hydrolyze the abscess proteins into amino acids.[29] The amino acid, alanine (Ala) has been suggested as a marker of meningiomas, a common extra-axial neoplasm of both humans and animals. Ala is commonly found in meningiomas, along with Lac, and is rarely found in other types of tumors.[1,71,72]

## $^{1}$H-MRS REGIONAL VARIABILITY

A study by Kaiser *et al. (*2005) that compared metabolites in older versus younger patients noted that independent of age, levels of Glu, NAA, Gln, and Cr were higher in the gray matter motor cortex compared with the corona radiata white matter.[54] Another study using high resolution MRSI of the frontal, occipital and parietal lobes determined that NAA and Cr were significantly higher in cortical gray matter than white matter in all regions studied.[73] The only significant regional difference found in this study was that the NAA/Cho ratio was higher in the occipital lobe, due to overall low Cho in this area. This is thought to be an important finding because decreased NAA/Cho ratios of neoplastic lesions in the occipital lobe may look like ratios found in normal brain of other regions.[73] In a study of the effects of normal aging, Pfefferbaum *et al.* (1999) determined that

the N-acetyl moiety (NAc) was higher in gray matter than white matter in younger and older subjects.[74] This and other characteristic spectral differences in white versus gray matter have been determined in a number of studies.[73,75-78] (See Table 1). Metabolite concentrations are similar in each of the studies, despite the use of differing techniques.[78] In general, higher metabolite concentrations were found in gray matter, especially Glu, when compared to white matter.[78] Cho is higher in white matter than cortical gray matter, while Cr levels are lower in white matter than gray matter.[1]

Table 1. Human regional brain $^{1}$H-MRS. Absolute metabolite concentrations (mM), concentration ratios and quality parameters in 12 healthy adult human controls (mean, SD). Weibenga *et al. (*2014).

| | White matter frontal | | | | White matter semioval | | | | White matter parietal | | | |
|---|---|---|---|---|---|---|---|---|---|---|---|---|
| | Baseline | | Follow-up | | Baseline | | Follow-up | | Baseline | | Follow-up | |
| tCr | 4.9 ± 0.8 | | 4.8 ± 0.9 | | 4.5 ± 0.7 | | 4.3 ± 0.8 | | 4.6 ± 0.7 | | 4.5 ± 0.8 | |
| tNAA | 7.8 ± 1.0 | | 7.8 ± 1.1 | | 8.2 ± 1.1 | | 8.0 ± 1.3 | | 8.2 ± 0.9 | | 8.0 ± 1.1 | |
| Cho | 1.6 ± 0.3 | | 1.6 ± 0.3 | | 1.5 ± 0.3 | | 1.4 ± 0.3 | | 1.4 ± 0.2 | | 1.4 ± 0.2 | |
| Ins | 3.9 ± 0.6 | | 3.9 ± 0.7 | | 3.5 ± 0.7 | | 3.4 ± 0.6 | | 4.1 ± 0.7 | | 3.9 ± 0.7 | |
| Glu | 6.1 ± 1.1 | | 6.3 ± 1.4 | | 4.7 ± 1.4 | | 4.8 ± 1.6 | | 5.0 ± 1.3 | | 5.0 ± 1.4 | |
| tNAA/tCr | 1.59 ± 0.19 | | 1.63 ± 0.20 | | 1.83 ± 0.20 | | 1.85 ± 0.17 | | 1.79 ± 0.17 | | 1.80 ± 0.17 | |
| Cho/tCr | 0.33 ± 0.04 | | 0.33 ± 0.04 | | 0.33 ± 0.03 | | 0.32 ± 0.03 | | 0.31 ± 0.04 | | 0.31 ± 0.05 | |
| Ins/tCr | 0.79 ± 0.11 | | 0.83 ± 0.20 | | 0.78 ± 0.14 | | 0.79 ± 0.15 | | 0.88 ± 0.12 | | 0.88 ± 0.16 | |
| Glu/tCr | 1.25 ± 0.16 | | 1.31 ± 0.25 | | 1.05 ± 0.23 | | 1.09 ± 0.28 | | 1.08 ± 0.23 | | 1.11 ± 0.22 | |
| FWHM | 5.6 ± 1.2 | | 5.4 ± 1.3 | | 5.0 ± 1.4 | | 4.9 ± 1.6 | | 4.9 ± 1.1 | | 4.8 ± 1.1 | |
| SNR | 11.9 ± 1.9 | | 11.9 ± 2.2 | | 11.9 ± 2.0 | | 12.0 ± 1.9 | | 13.4 ± 2.0 | | 14.1 ± 2.3 | |
| | Gray matter frontal | | | | Gray matter parietal | | | | | | | |
| | Baseline | | Follow-up | | Baseline | | Follow-up | | | | | |
| tCr | 6.7 ± 1.0 | | 6.1 ± 1.1 | | 5.8 ± 0.8 | | 6.2 ± 1.0 | | | | | |
| tNAA | 8.0 ± 1.1 | | 7.7 ± 1.2 | | 8.3 ± 1.0 | | 8.7 ± 1.3 | | | | | |
| Cho | 1.8 ± 0.3 | | 1.8 ± 0.3 | | 1.0 ± 0.2 | | 1.1 ± 0.2 | | | | | |
| Ins | 5.2 ± 0.7 | | 4.9 ± 0.8 | | 4.6 ± 0.5 | | 4.6 ± 0.7 | | | | | |
| Glu | 9.5 ± 1.4 | | 8.8 ± 1.9 | | 8.3 ± 1.5 | | 8.6 ± 1.9 | | | | | |
| tNAA/tCr | 1.19 ± 0.10 | | 1.27 ± 0.12 | | 1.43 ± 0.13 | | 1.41 ± 0.13 | | | | | |
| Cho/tCr | 0.28 ± 0.02 | | 0.29 ± 0.03 | | 0.17 ± 0.02 | | 0.18 ± 0.02 | | | | | |
| Ins/tCr | 0.78 ± 0.09 | | 0.81 ± 0.10 | | 0.79 ± 0.10 | | 0.76 ± 0.09 | | | | | |
| Glu/tCr | 1.43 ± 0.18 | | 1.43 ± 0.17 | | 1.42 ± 0.15 | | 1.38 ± 0.14 | | | | | |
| FWHM | 7.3 ± 1.2 | | 6.9 ± 1.7 | | 5.4 ± 1.5 | | 5.9 ± 1.5 | | | | | |
| SNR | 9.3 ± 1.5 | | 9.4 ± 1.2 | | 13.6 ± 2.2 | | 14.0 ± 2.2 | | | | | |

## $^{1}$H-MRS IN SPECIFIC CNS DISEASES

### BRAIN TUMORS

Numerous studies have used $^{1}$H-MRS in the diagnosis and grading of brain tumors, differentiating types of brain tumors, determining brain tumor margins and monitoring response to treatment in humans.[2,17,18,32,48,49,53,79-93] In a study by Fountas *et al.* (2000), comparing MRS to MRI and histopathologic diagnoses of brain tumors, MRS was successful in establishing a correct diagnosis of tumor type in 85.6% of the population, whereas standard MRI was correct in 78% of the cases.[82]

A study using MRSI in conjunction with perfusion MRI enabled the differentiation between metastatic lesions, lymphoma and glioblastoma multiforme, with high specificity.[80]

$^{1}$H-MRS, capable of differentiating tumor types, can facilitate diagnosis, treatment and follow-up of brain tumors without the use of invasive biopsy techniques. Numerous studies on brain tumor $^{1}$H-MRS have determined that brain tumors, in general, exhibit decreased levels of NAA and increased levels of Cho, causing a decrease in the NAA/Cho ratio.[52,53] These findings are thought to be due to the absence of normal neuronal tissue and increased membrane turnover.[1] Extra-axial tumors such as meningiomas will have significantly decreased levels of NAA or lack the peak completely because of their non-neuronal origin.[16,17 30]

Other changes, such as increased Lac and lipid may be evident due to alterations in metabolism (i.e. anaerobic glycolysis) or due to necrosis or ischemia associated with tissue damage and areas of decreased blood supply.[52] Increased levels of myoinositol (mI) are detected when short TE techniques are used.[1,72] This is thought to be due to increased number of glial cells, especially in tumors such as high grade gliomas.[22,85]

A study that used MRSI in differentiating brain diseases in children found that high-grade tumors had a 60% lower NAA/Cho ratio, 50% higher Cho/Cr ratio and a 43% lower NAA/Cr ratio than non-neoplastic lesions. This same study found that low-grade neoplasms had a 50% higher Cho/Cr ratio than non-neoplastic lesions as well.[85] Other studies have demonstrated similar findings suggesting that high-grade tumors will have higher Cho levels and therefore lower NAA/Cho levels than low -grade tumors.[85,88] In addition, high-grade tumors can exhibit higher Lac levels than low-grade tumors.[88] Another study using preoperative, high spatial resolution (using a nominal voxel size of 0.45 $cm^3$) MRSI to grade gliomas determined that there were significantly lower total NAA values, higher Cho values and higher Cho/NAA ratios for grade III gliomas when compared to grade II glial tumors.[89] This study also determined that $^1$H-MRS spectra from grade III astrocytomas had significantly higher maximum Cr values, when compared with grade III oligodendrogliomas and grade III oligoastrocytomas in human patients. This higher maximum Cr concentration in grade III astrocytomas may be due to the increased energy metabolism and

increased growth rate of the high-grade tumors.[89] The Cho/PCr-Cr ratio has been shown to be a reliable marker for tumor grade identification. The Cho/PCr-Cr ratio was 2.05 +/- 0.18 in low-grade astrocytomas, 2.58 +/- 0.11 in grade III and 5.1 +/- 0.89 in grade IV. [82] These are typical examples, where $^{1}$H-MRS studies have used the ratios of NAA, Cho and Cr to diagnose and differentiate brain lesions. A study by Vuori *et al.* (2004) determined that while total Cho and Cr values helped differentiate astrocytomas from oligodendrogliomas and oligoastrocytomas, none of the metabolite ratios NAA/Cho, NAA/Cr, and Cho/Cr helped differentiate the tumor types.[94]

The use of metabolite ratios may result in loss of metabolic information, since a ratio may not change when both the numerator and the denominator change, and the ratio does not reveal the direction of the changes. Furthermore, it may not take into account regional and age-dependent differences in metabolite signals. A study by McKnight *et al.* (2001) used 3-D CSI to establish a linear model of total Cho versus NAA, in the form of a Gaussian z-score. The Cho to NAA Index (CNI) indicates the number of standard deviations of difference between amount of Cho and NAA at a voxel location and mean values of control spectra. Spectra from normal, edematous, and necrotic regions will have CNIs close to zero, whereas those recorded from a tumor are elevated. A CNI of 2.0 was used as a threshold to determine tumor versus peri-tumoral tissue.[51] This technique may increase the likelihood of directing a biopsy towards the area of the highest probability of being malignant and aid in surgical resection

of all neoplastic tissue, while sparing normal tissue. This same group performed a follow-up experiment using the CNI to compare contrast-enhancing versus non-contrast enhancing areas associated with gliomas that were hyperintense on T2 weighted MRI images.[95] This study confirmed the original data; the CNIs of biopsy samples not containing tumors were significantly different from those obtained within tumors. Using the previously determined CNI of 2.0 as the threshold, tumors were distinguished from non-tumor with 96% sensitivity and 57% specificity. But when a CNI of 2.5 was used instead, the sensitivity and specificity were 90% and 86%, respectively.[95] It was also determined that 50% of biopsy specimens from contrast-enhancing tumors (n=42) positively identified as tumor with histopathology came from non-enhancing portions of the lesions. Additionally 36% to 45% of the hyperintense lesions that did not enhance on contrast-enhanced T1 -weighted MR images were suspicious for tumor cells, based on the CSI spectra and CNI of greater than 2.5.[95] Unfortunately, histopathology was not available for the confirmation of these regions. $^{1}$H-MRS is a robust tool for differentiating brain tumor tissue from peri-tumoral edema, necrosis and normal tissue because of the high sensitivity to metabolic changes that may not be evident with conventional MRI.

STROKE

The most consistent findings with $^{1}$H-MRS after cerebral infarction in humans and animals are an elevated Lac and a decrease in NAA.[1,96-98] An initial

decrease in Cr, mI and choline Cho have also been noted in some studies, but not usually with statistical significance.[31,98,99] An early study by Graham *et al.* (1993) showed that on $^{1}$H-MRS scans performed within 60 hours of acute stroke, all patients had significant elevation in Lac. Follow-up scans performed seven to seventeen days after onset of clinical signs had an average decrease in maximum Lac peak of 36% per week.[99] A study by Kang *et al.* (2009) performed experimental middle cerebral artery occlusion (MCAO) in laboratory beagles, and demonstrated significantly increased Lac three days after the ischemic event. Ten days after MCAO, Lac levels were further increased when compared to the initial $^{1}$H-MRS scan.[31] The key difference to note between these two studies is that the human study performed follow-up $^{1}$H-MRS weeks after the ischemic event, whereas the canine study performed the follow-up scan ten days after the ischemic event. The decline in Lac after the acute ischemic period noted in the human study may be due to diffusion of lactate in to the bloodstream, dissolution of necrotic cells and reperfusion of tissues.

Graham *et al.* (1993) also determined that the size of the ischemic lesion had a positive correlation with average measurable Lac and the maximum lesion Lac on initial presentation, but on follow-up $^{1}$H-MRS, there was no correlation between lesion size and measurable Lac.[99] It is thought that 48 to 72 hours after cerebral infarction, leukocyte infiltration in the infarcted zone likely contributes to the persistent lactate levels noted on follow-up MR spectroscopy. Since Lac is known to rise within minutes of acute ischemia, it may serve as a useful marker

of subacute and acute ischemic injury, before abnormalities are noted with conventional MRI.

Numerous studies have demonstrated that $^{1}$H-MRS, used in conjunction with diffusion weighted images (DWI) may aid in the diagnosis and monitoring of stroke.[100,101] Parsons *et al.* (2000) showed that when using the combination of acute Lac/Cho ratio on $^{1}$H-MRS and DWI lesion volume, there were improved prediction outcome in all cases.[100]

NAA is another useful marker of ischemic injury. It is generally thought that NAA declines slowly over a time frame of hours after an ischemic event.[1] The 1993 study by Graham *et al.* determined that in acute ischemia, NAA was significantly decreased in eight out of ten human subjects, when compared to the contralateral, non-affected hemisphere. It was also shown that NAA continued to decrease by an average of 29% per week between initial scans and follow-up $^{1}$H-MRS.[99] It was thought that delayed decrease in NAA may indicate late death of neurons within the ischemic penumbra, the tissue area surrounding the ischemic core that is exposed to less severe degree of perfusion reduction.[99] In the canine MCAO study by Kang *et al.* (2009), there were significantly decreased $^{1}$H-MRS NAA concentration in the acute stage, but ten days after the onset of ischemia, NAA levels were already significantly recovered.[31] This may indicate functional recovery of previously damaged neurons.

TRAUMATIC BRAIN INJURY (TBI)

Conventional MRI has been shown to be highly sensitive for the detection of hemorrhagic and non-hemorrhagic contusions, and is useful for the monitoring of edema, mid-line shift, atrophy and lesions of post-traumatic epilepsy in humans. However, with early brain trauma, a damaging cascade of cellular damage, ion-channel mediated neurotransmitter release, oxidative damage and altered cellular metabolism and perfusion cause the clinical manifestations of TBI. These and other microscopic changes may not be detectable with MRI.[102] Humans with a very low Glasgow Coma Scale (GCS) of <5 may exhibit no abnormalities with standard MRI evaluation on admission. Therefore, other imaging modalities have been used in conjunction with standard MRI sequences in the diagnosis and monitoring of traumatic brain injury.[1] Multiple studies have indicated that $^{1}$H-MRS is sensitive for the detection of micro-structural and metabolic changes associated with TBI, when standard MRI is normal.[58,102,103]

Holshouser *et al.* (2005) demonstrated a reduction in NAA and increase in Cho in 40 children with moderate to severe TBI.[58] Similar findings have been noted in numerous $^{1}$H-MRS studies of TBI in children [104-106] and adults.[103,107,108] It has been determined that there is a significant correlation between the decrease in NAA, increase in Cho and the severity of the injury.[103,104] As in children, diffusely reduced NAA in adult humans may serve as an early indicator of diffuse axonal injury (DAI). Cho is a breakdown product of membrane disruption, therefore increased levels observed after TBI have been attributed to DAI. [58,105]

Aaen *et al.* (2010) found that in children with non-accidental TBI, mean total NAA/Cho and NAA/Cr ratios were significantly lower in patients with poor outcomes.[106] In addition, elevated Lac levels were more commonly noted in children with a poor outcome (83% of 12), when compared to those with a good outcome (38% of 32).[106] Non-accidental TBI in children tends to be associated with more severe brain injury, when compared to accidental trauma and may more closely resemble traumatic brain injury seen in veterinary medicine (e.g. hit by car). Another study of TBI in children found that elevated Lac was noted in 91% of infants and 80% of children with a poor outcome and was not found to be elevated in any of the patients with a good clinical outcome.[104] Changes in Lac levels are less common in adult patients with traumatic brain injury.[103,105]

Elevated Glx has also been shown to be elevated in people with TBI. A study by Ashwal *et al.* (2004) showed elevations in Glx in the occipital lobe of children after traumatic brain injury when compared to controls, but there was no difference between those individuals with poor outcomes compared with a good outcome.[109] Another study by Ashwal *et al.* (2004) determined that after a mean of 7 days following TBI in children, occipital lobe mI was significantly increased compared with controls. Patients with higher mI levels had poorer outcomes 6-12 months after sustaining injury.[110] The reason for this elevation is thought to be due to astrogliosis or disturbances in osmotic function.

## INFECTIOUS, INFLAMMATORY AND DEMYELINATING LESIONS

Infectious, inflammatory and demyelinating brain lesions may be difficult to differentiate and $^{1}$H-MRS has been shown to contribute additional information when there is uncertainty about these lesions noted with standard MRI.[1,111] This is of the utmost importance when dealing with intracranial infections, because they can progress rapidly and may be life threatening.

Brain abscesses may resemble cystic mass-like lesions of varying etiology with standard MRI.[1,112] Bacterial abscesses are necrotic lesions and are lacking normal brain metabolites such as NAA, Cho and Cr.[29] Specific resonance peaks are commonly identified within the core of a pyogenic brain abscess: succinate (Suc) at 2.40 ppm, acetate (Ac) at 1.92 ppm, alanine (Ala) a doublet centered at 1.47 ppm, amino acids (valine, leucine and isoleucine) resonating at 0.90 ppm, as well as lipids 0.90 ppm and 1.30 ppm and Lac at 1.33 ppm.[1,29,113]

A study by Garg *et al.* (2004) showed promising results in differentiating abscesses resulting from anaerobic bacteria from those of aerobic bacteria or sterile abscesses.[112] The study showed that signals from Suc and/or Ac were associated with aerobic infections, suggestive of enhanced glycolysis and fermentation. Sterile abscesses had variable resonance characteristics, likely due to prior bacterial infection that was effectively treated with antibiotics.[112] These findings were corroborated in a similar study by Pal *et al.* (2010). In this study, it was also determined that resonances from amino acids were present in 80% of pyogenic brain abscesses, with a sensitivity of 0.72, specificity of 0.30, positive

predictive value of 0.80 and negative predictive value of 0.20, for the diagnosis of pyogenic brain abscesses.[29] Abscesses contain large amounts neutrophils and protein. Proteolytic enzymes that are released with the breakdown of neutrophils are thought to hydrolyze proteins into amino acids. In the cases where amino acids were not identified with ex vivo $^{1}$H-MRS of brain abscesses, it is thought to be due to decreased inflammation and therefore decreased neutrophil breakdown.[29]

A study by Luthra *et al.* (2007) used $^{1}$H-MRS in conjunction with conventional MRI and DWI to differentiate pyogenic brain abscesses from those due to fungal or tubercular infections. All of the abscesses, regardless of etiology, were hyperintense on T2-weighted images, hypointense on T1-weighted images, and exhibited well-defined rim enhancement on post-contrast images. A distinguishing feature noted with fungal abscesses were intra-cavitary projections from the abscess wall that were absent from pyogenic and tubercular abscesses. DWI findings were not consistently significantly different between the abscess groups. In vivo $^{1}$H-MRS of pyogenic abscesses in this study showed findings similar to the previously mentioned studies: increased amino acids in 89/91 of pyogenic abscesses, Lac in 46/91, lipid with Lac in 45/91, Ac in 25/91 and Suc in 46/91. All 11 of the tubercular abscesses contained lipid resonance peaks. Four of eight fungal abscesses contained amino acids and Lac, three contained lipids with Lac and one showed a peak from lipid solely. Interestingly, multiple signals between 3.6 ppm and 3.8 ppm were noted, consistent with trehalose within the

fungal wall.[113] The findings in this study indicate that $^{1}$H-MRS, in conjunction with conventional MRI, may be important in the diagnoses and appropriate treatment of different types of brain abscesses.

Another important inflammatory disease of humans that has been widely studied with $^{1}$H-MRS is multiple sclerosis (MS), an autoimmune disorder that leads to inflammation, demyelination, and chronic sclerotic brain plaques. The most consistent findings associated with MS plaques are decreased NAA, that is likely due to neuronal and axonal injury and increased Cho, which is thought to be associated with cell membrane turnover and increased steady-state levels of membrane phospholipids during myelin breakdown and remyelination.[1,114]

A study by Mader *et al.* (2000) followed MS patients in a placebo group and those administered an immunomodulatory drug over two years, and compared them to healthy volunteers. During the acute stages of a newly formed plaque, Cho was significantly increased relative to that of healthy volunteers. Also, the NAA/Cho and NAA/Cr ratios were significantly decreased. Cr levels were negatively correlated with contrast enhancing plaque size. Over time, NAA levels were variable but were significantly reduced after one month in MS patients and gradually increased back to normal levels after two years. Cr and Cho levels remained elevated over a year, but declined to near-normal levels over 2 years.[42] It is thought that the persistent elevations in Cr, may be due to gliosis and that the variable recovery of NAA over time may be related to reversible metabolic changes or resolution of edema. In large, acute

demyelinating lesions, elevations in Lac may also be present and likely represent the metabolism of inflammatory cells. There may also be a transient elevation in lipid, due to the breakdown of myelin sheath and engulfment of lipid debris by macrophages.[1,114]

An important aspect of $^{1}$H-MRS in MS imaging is the metabolic changes detected in white matter that is normal in appearance with conventional MR imaging.[115] A study by Leary *et al.* (1999) determined that in patients with primary progressive MS, though there were minimal changes on conventional MRI studies, the absolute concentration of NAA and the NAA ratios were significantly reduced in the normal appearing white matter in these patients when compared to age-matched controls.[116] NAA decreases found in normal-appearing white matter have been attributed to axonal damage and loss.[1] This finding is an important concept for many disease processes, because $^{1}$H-MRS has the potential to identify disease earlier and at different phases, that may not be identifiable using conventional imaging modalities.

## BRAIN 1H-MRS IN VETERINARY MEDICINE

Early canine brain $^{1}$H-MRS studies were mostly ex vivo studies or focused on finding models for human diseases such as ischemic brain injury[31,117,118] and brain tumors[79,119,120] More recent canine brain $^{1}$H-MRS research has focused on utilizing this imaging modality for the diagnosis, monitoring, and treatment of diseases of clinical relevance to veterinary medicine.[121-125] The first study to

establish the feasibility of performing canine brain $^{1}$H-MRS by Martin-Vaquero *et al. (*2012). They acquired SVMS $^{1}$H-MRS spectra from the parietal cortex and cortical-ventricular area of four healthy Beagle dogs using 1.0 $cm^3$ and 8.0 $cm^3$ voxel sizes respectively at 3.0 T and 7.0 T field strengths.[122] They were able to identify NAA, Cho, and Cr consistently at 3.0 T, but only in two of four dogs using 7.0 T. This was thought to be due to insufficient water suppression, resulting in excessive field inhomogeneity.[122] No metabolite concentrations were quantified, as this was not the objective of the study.

In 2013, Ober *et al.* attempted to develop a canine brain $^{1}$H-MRS protocol with maximal image quality, while maintaining a reasonable scan time.[123] They tested SVMRS and MRSI protocols at short (35 ms) and long (144 ms) TEs. SVMRS were acquired using 1 $cm^3$, 4 $cm^3$, 8 $cm^3$ and 27 $cm^3$ voxel volumes with a NEX of 8. MRSI acquisitions were obtains with a 1 cm VOI thickness, using 12 x 12, 18 x 18, and 24 x 24 matrices with a NEX of 1. All VOIs, for the various parameters, were centered on the interthalamic adhesion. They evaluated each scan subjectively and qualitatively. No attempts at metabolite quantification were made. They determined that with SVMRS, spectrum quality subjectively improved with increasing VOI, but voxel volumes greater than 1 $cm^3$ incorporated too many tissue types to compare specific brain regions. The 1 $cm^3$ voxel produced non-diagnostic spectra. The spectrum quality of the MRSI was similar to those achieved using the SVMRS voxel sizes of 4 $cm^3$ and 8$cm^3$. The 12 x 12 matrix resulted in decreased quality spectra and due to the decreased spatial resolution,

had decreased voxel specificity. There was no significant difference in the subjective quality of the 18 x 18 and 24 x 24 matrix sizes, but the latter resulted in a longer scan time (9 minutes and 40 seconds) compared to the former (5 minutes and 28 seconds).[123] They also noted poor quality MRSI spectra when the VOI was placed with the edges outside of the brain parenchyma due to prominent lipid peaks, despite the use of saturation bands. The spectra obtained with the VOI placed entirely within the brain had decreased baseline noise, less prominent lipid peaks and consistent identification of metabolite peaks.[123] However, using this technique, parenchyma along the periphery of the brain, adjacent to the calvarium would be excluded, as a result of a rectangular VOI within a structure with rounded margins. They also noted significantly higher quality spectra when using long TE (144ms) scans. Additionally, using this TE allowed the identification of an inverted lactate peak, when present.[123] Using a long TE, however, only allows identification of metabolites with a long transverse relaxation times.

A study by Warrington *et al.* (2013) was the first to report relative metabolite concentrations and ratios of canine brain $^{1}$H-MRS using a protocol established by Ober *et al. (*2013) at 3.0 T using TEs of 35 and 144 ms. They used a 20 cm FOV, an 18 x 18 matrix, and 1cm thick voxels with a resultant voxel volume of 1.23 $cm^3$ and a scan time of 328 seconds.[124] $^{1}$H-MRS was performed in six locations: centered on the olfactory bulbs, the rostral edge of the corpus

callosum, the interthalamic adhesion, the rostral aspect of the cerebellum and centered on the brainstem.[124] Their results are in Table 2.

**Table 2**. Regional 1H-MRS in healthy dogs at a TE of 144ms. Peak height (MR units) for metabolites and metabolite ratios in 10 clinically normal dogs. Warrington *et al.* (2013).

| Lobe | Variable | Mean | Median | Minimum | Maximum |
|---|---|---|---|---|---|
| Olfactory bulb (n = 23) | NAA | 2,206.3 | 2,200.0 | 1,496.0 | 2,884.0 |
| | Choline | 1,918.4 | 1,842.0 | 1,096.0 | 3,102.0 |
| | Creatine | 1,607.3 | 1,668.0 | 880.0 | 2,136.0 |
| | NAA-to-choline ratio | 1.214 | 1.257 | 0.751 | 1.846 |
| | NAA-to-creatine ratio | 1.395 | 1.298 | 1.029 | 1.933 |
| | Choline-to-creatine ratio | 1.187 | 1.174 | 0.824 | 1.660 |
| Frontal (n = 82) | NAA | 2,312.1 | 2,136.0 | 732.0 | 4,554.0 |
| | Choline | 2,719.6 | 2,637.0 | 1,236.0 | 4,485.0 |
| | Creatine | 1,874.2 | 1,775.0 | 552.0 | 3,591.0 |
| | NAA-to-choline ratio | 0.849 | 0.815 | 0.469 | 1.213 |
| | NAA-to-creatine ratio | 1.245 | 1.209 | 0.944 | 1.810 |
| | Choline-to-creatine ratio | 1.512 | 1.467 | 1.035 | 3.201 |
| Parietal (n = 48) | NAA | 5,253.9 | 4,944.0 | 2,079.0 | 9,345.0 |
| | Choline | 3,692.8 | 3,538.5 | 1,680.0 | 6,100.0 |
| | Creatine | 2,841.6 | 2,595.0 | 861.0 | 4,844.0 |
| | NAA-to-choline ratio | 1.427 | 1.383 | 1.062 | 2.078 |
| | NAA-to-creatine ratio | 1.878 | 1.828 | 1.394 | 2.919 |
| | Choline-to-creatine ratio | 1.333 | 1.281 | 0.993 | 2.008 |
| Thalamus (n = 96) | NAA | 6,891.0 | 6,893.5 | 3,606.0 | 11,802.0 |
| | Choline | 6,823.9 | 6,925.0 | 3,370.0 | 11,304.0 |
| | Creatine | 4,760.8 | 4,735.5 | 2,350.0 | 8,008.0 |
| | NAA-to-choline ratio | 1.029 | 1.003 | 0.804 | 1.598 |
| | NAA-to-creatine ratio | 1.456 | 1.456 | 1.155 | 1.755 |
| | Choline-to-creatine ratio | 1.429 | 1.423 | 1.017 | 1.708 |
| Temporal (n = 96) | NAA | 4,615.7 | 4,650.0 | 1,364.0 | 8,785.0 |
| | Choline | 3,680.0 | 3,661.5 | 872.0 | 7,315.0 |
| | Creatine | 2,987.9 | 2,958.0 | 1,108.0 | 5,526.0 |
| | NAA-to-choline ratio | 1.294 | 1.262 | 0.796 | 2.318 |
| | NAA-to-creatine ratio | 1.559 | 1.537 | 1.145 | 2.167 |
| | Choline-to-creatine ratio | 1.240 | 1.212 | 0.787 | 1.838 |
| Piriform (n = 24) | NAA | 3,272.8 | 3,034.5 | 2,180.0 | 5,330.0 |
| | Choline | 3,179.0 | 3,210.0 | 1,458.0 | 4,875.0 |
| | Creatine | 2,422.1 | 2,438.0 | 1,470.0 | 3,485.0 |
| | NAA-to-choline ratio | 1.069 | 1.113 | 0.687 | 1.568 |
| | NAA-to-creatine ratio | 1.352 | 1.328 | 0.984 | 1.818 |
| | Choline-to-creatine ratio | 1.298 | 1.333 | 0.947 | 1.797 |
| Occipital (n = 48) | NAA | 4,907.0 | 4,814.0 | 2,526.0 | 8,010.0 |
| | Choline | 3,160.1 | 3,077.5 | 1,604.0 | 5,328.0 |
| | Creatine | 3,123.5 | 3,095.0 | 1,719.0 | 5,530.0 |
| | NAA-to-choline ratio | 1.563 | 1.564 | 1.263 | 2.193 |
| | NAA-to-creatine ratio | 1.583 | 1.569 | 1.301 | 1.936 |
| | Choline-to-creatine ratio | 1.022 | 1.031 | 0.791 | 1.262 |
| Cerebellum (n = 91) | NAA | 3,371.5 | 3,112.0 | 693.0 | 7,446.0 |
| | Choline | 2,990.7 | 2,890.0 | 459.0 | 5,940.0 |
| | Creatine | 2,775.6 | 2,492.0 | 540.0 | 5,934.0 |
| | NAA-to-choline ratio | 1.127 | 1.092 | 0.665 | 1.842 |
| | NAA-to-creatine ratio | 1.214 | 1.191 | 0.727 | 1.842 |
| | Choline-to-creatine ratio | 1.100 | 1.079 | 0.728 | 1.719 |
| Brainstem (n = 48) | NAA | 2,691.0 | 2,736.0 | 1,248.0 | 4,176.0 |
| | Choline | 2,409.6 | 2,369.5 | 1,152.0 | 3,552.0 |
| | Creatine | 1,987.8 | 1,946.0 | 552.0 | 3,340.0 |
| | NAA-to-choline ratio | 1.127 | 1.168 | 0.612 | 1.598 |
| | NAA-to-creatine ratio | 1.400 | 1.378 | 0.916 | 2.866 |
| | Choline-to-creatine ratio | 1.281 | 1.207 | 0.825 | 2.542 |

n = Number of voxels on which numeric data are based.

Ono *et al.* (2014) studied regional variations and age-related changes detectable with brain SVMRS in 15 healthy Beagle dogs at 1.5 T. 3.4 $cm^3$ voxels were placed on mid-line over the frontal lobes, midline of the occipital lobes and centrally in the cerebellum. The PRESS SVMRS technique was used, with a NEX of 256 for improved SNR, with resultant scan times of 8.53 minutes per region. They found that Cho/Cr was significantly higher in young dogs, when compared to other age groups. NAA/Cho was significantly lower in young and geriatric dogs, when compared to the adult dogs. Regional variability noted was in the frontal lobe, which had significantly higher Cho/Cr and significantly lower NAA/Cho and in the cerebellum, which had significantly lower NAA/Cr compared to other regions.[125] A similar study in humans found that the NAA/Cho ratio was higher in the occipital lobe, due to overall low Cho.[73] The relatively lower NAA/Cr in the cerebellum may correspond to increased cerebellar Cr seen in humans.[1] Ono *et al.* (2014) results are reported in Tables 3 and 4.

Table 3. Area under the $^1$H-MRS metabolite peak in three brain regions of healthy Beagles. Four metabolites in three brain regions grouped according to age. Areas are reported as mean and standard deviation. Ono *et al.* (2014).

| Group and anatomic region | *N*-acetyl aspartate | Creatine | Choline | Lactate-alanine |
|---|---|---|---|---|
| Young | | | | |
| Frontal lobe | 105.37 ± 7.03 | 70.93 ± 6.35 | 164.21 ± 10.21 | 7.04 ± 7.04 |
| Occipital lobe | 115.85 ± 4.24 | 55.51 ± 1.88 | 129.91 ± 8.21 | ND |
| Cerebellum | 100.29 ± 5.03 | 74.03 ± 5.18 | 122.82 ± 3.11 | ND |
| Adult | | | | |
| Frontal lobe | 62.43 ± 3.76 | 36.74 ± 4.22 | 69.13 ± 2.86 | 1.80 ± 1.24 |
| Occipital lobe | 90.17 ± 6.34 | 60.64 ± 2.94 | 73.67 ± 3.30 | 2.54 ± 2.54 |
| Cerebellum | 98.65 ± 3.84 | 71.37 ± 3.46 | 84.11 ± 8.57 | ND |
| Geriatric | | | | |
| Frontal lobe | 44.28 ± 8.26 | 30.66 ± 4.37 | 59.48 ± 7.81 | ND |
| Occipital lobe | 80.70 ± 6.58 | 56.74 ± 0.40 | 76.00 ± 4.57 | ND |
| Cerebellum | 81.4 ± 5.03 | 62.26 ± 8.50 | 71.36 ± 7.46 | 9.66 ± 4.31 |

Table 4. Metabolite ratios for three brain regions in healthy Beagles. Metabolites are reported as mean and standard deviation. Ono *et al.* (2014).

| Group and anatomic region | *N*-acetyl aspartate-to-creatine ratio | Choline-to-creatine ratio | *N*-acetyl aspartate to choline ratio | Lactate-alanine-to-creatine ratio |
|---|---|---|---|---|
| Young | | | | |
| Frontal lobe | 1.52 ± 0.25 | 2.39 ± 0.53 | 0.64 ± 0.07 | 1.41 ± 1.41 |
| Occipital lobe | 2.11 ± 0.34 | 2.35 ± 0.35 | 0.91 ± 0.15 | ND |
| Cerebellum | 1.37 ± 0.14 | 1.70 ± 0.33 | 0.81 ± 0.10 | ND |
| Adult | | | | |
| Frontal lobe | 1.82 ± 0.66 | 2.07 ± 0.95 | 0.90 ± 0.10 | 0.05 ± 0.03 |
| Occipital lobe | 1.50 ± 0.18 | 1.21 ± 0.06 | 1.23 ± 0.11 | 0.05 ± 0.05 |
| Cerebellum | 1.40 ± 0.21 | 1.18 ± 0.23 | 1.21 ± 0.24 | ND |
| Geriatric | | | | |
| Frontal lobe | 1.43 ± 0.11 | 2.00 ± 0.25 | 0.74 ± 0.06 | ND |
| Occipital lobe | 1.42 ± 0.11 | 1.34 ± 0.07 | 1.08 ± 0.11 | ND |
| Cerebellum | 1.40 ± 0.21 | 1.30 ± 0.13 | 1.17 ± 0.08 | 0.12 ± 0.05 |

For the most part, general anesthesia is a requirement for performing MRI and $^{1}$H-MRS in veterinary patients. In some cases, scans can be performed under heavy sedation. The only exception is for patients in a comatose or severely moribund state, where scans may be performed without sedation or anesthesia. Lee *et al.* (2010) demonstrated that there are significant alterations in certain brain metabolite levels when patients are administered ketamine or pentobarbitol.[121] Glx, Cr and NAA levels were significantly lower in the group of dogs that received pentobarbital when compared to the ketamine group.[121] This is something to be taken into consideration when devising anesthetic protocols for establishing normal MR spectra for certain brain regions and when comparing pathologically affected areas to what is considered normal.

## IMPACT OF VOXEL SIZE

The brain parenchyma and surrounding non-osseous structures of the calvarium are predominantly composed of water and adipose tissue. In MRI, it is the intrinsic molecular qualities of water and fat that provide signal to create an image. In $^{1}$H-MRS applications, it is predominantly small metabolite signals, such as NAA and Cho that are of interest. The chemical shift characteristics of these small brain metabolites are of the utmost importance in $^{1}$H-MRS, because this allows distinction of one metabolite from another.[1] As previously mentioned, these small brain metabolites are in the order of approximately 1-30 mM, which is approximately 100,000 times less than that of water or fat.[2] Spectral resolution is significantly determined by magnetic field strength. Recognition of individual metabolites, via separation of the metabolite peaks, increases linearly with magnetic field strength.[8] With 3.0 T and higher magnetic field strengths in particular, there is improved SNR (signal to noise ratio). This is critical for allowing spectra to be obtained from smaller and/or more discrete volumes of tissue.[2]

A study by Christiansen *et al.* (1993) used a $^{1}$H-MRS phantom to compare the $^{1}$H-MRS signal strength produced when using different voxel sizes. They showed that a linear relationship exists between the resultant signal strength and the size of the volume of interest (VOI), ranging from 8-64 cm$^{3}$, for NAA and water.[126] Gideon *et al. (*1992) demonstrated regional variation within a visibly infarcted region of brain in humans.[45] They analyzed a larger (18-27 ml) volume

of interest within the infarct as well as a smaller VOI of 8mls (2 $cm^3$ x 2 $cm^3$ x 2 $cm^3$) placed within the center of the first VOI. The results of the study indicated that even though the NAA concentration was decreased within both voxels placed within the infarcted brain tissue, the smaller central voxel contained significantly less NAA than the outer region in five out of six patients in the acute phase and two to four weeks after the incident.[45] This finding may be attributed to a heterogeneous distribution of metabolites within lesions visualized with standard MRI, but also may be attributable to contamination of the outer voxel from adjacent normal tissue. Analysis of variability within lesions or of small structures (e.g. brain tissue of veterinary patients) clearly benefit from utilizing smaller voxels, while maintaining sufficient SNR to accurately identify and resolve each metabolite within the spectra.

Smaller voxels contain smaller amounts of tissues, fewer spins or nuclei to contribute to signal, and therefore produce lower SNR. Increasing the magnetic field strength to approximately 7.0 T or even 9.0 T will increase the signal acquired. However, the common field strengths used for clinical brain $^1$H-MRS studies in humans and animals are 1.5 T, 3.0 T and sometimes 7.0 T.

A method commonly utilized for acquiring sufficient signal in small regions of interest is to increase the number of averages (NEX). If the NEX is doubled, then the SNR will increase by the square root of 2 (i.e. 1.4).[1] Increasing the SNR cannot occur without a cost. As NEX increases, so does the overall scan time. This relationship is linear; doubling the NEX will double the scan time.[4] Factors

that affect scan time include repetition time (TR), phase matrix and the number of excitations (NEX). A typical TR time used in $^{1}$H-MRS is 1 to 2 seconds. It is important to have a sufficiently long TR time (> 5 x T1 relaxation of brain metabolites) for magnetization to fully recover before the next measurement. Matrix size is negligible with SVMRS but is variable with MRSI, depending on the volume of tissue that is being imaged. Therefore, although the NEX is the simplest parameter to adjust in order to improve the signal to noise ratio, it can result in $^{1}$H-MRS scans that are too long to be reasonably used in a clinical setting.[1]

Numerous mouse and rat brain $^{1}$H-MRS studies have been performed using very small voxel volumes, but at the expense of scan times. A study by van der Toorn *et al.* (1996) performed rat brain $^{1}$H-MRS using VOI of 3.6 x 3.5 x 3.6 mm in size (x-, y- and z-direction, respectively; total voxel volume of 0.04536 $cm^3$) using a 4.7 T magnet.[127] A NEX of greater than 128 and a scan time of approximately 40 minutes was required for each scan.[127] Another study by Tkac *et al.* (2003) compared several brain regions via SVMRS in different age neonatal rats using a 9.4 T magnet. They achieved even smaller VOI and sufficient SNR, but within 100 minute scan times.[27] In the hippocampus the VOI started as small as 2.5 x 1.5 x 3.0 mm, in the striatum from 3.0 x 2.0 x 3.0 mm and in the cerebral cortex using a VOI as small as 4.0 x 1.5 x 3.0 mm (i.e. 1.8 $cm^3$ voxel volumes).[27] In 2009, a study by Lei *et al.* successfully resolved 21 metabolites from the hippocampus and hypothalamus of mouse brains using a 14.1 T magnet. With

voxel sizes of approximately 0.08 mm x 0.08 mm x 0.6 mm, very high spatial resolution in the hippocampus and hypothalamus were reproducibly accomplished. A NEX of 320 to 480 were used to obtain adequate SNR resulting in 30-40 minute scan times.[128] These studies with stronger magnetic field strengths (e.g. 7.0, 9.0 and 14.1 T) are able to use smaller voxel sizes because signal increases proportionately to magnetic field strength.[4]

Title: MATERIALS AND METHODS

## ANIMALS

Eight intact female research dogs between 1 and 2 years of age were used in this study. All of the dogs were determined to be healthy. Specifically, none had a history of neurologic disease nor possessed any detectable neurologic deficits based on the examination of a board certified veterinary neurologist. They were housed on-site. All dog handling and procedures were conducted with the approval of the Institutional Animal Care and Use Committee (IACUC) of the University of Georgia.

For the MRI procedure, food was withheld for 12 hours prior to anesthesia. Water was withheld the morning of anesthesia. The dogs were pre-medicated with butorphanol tartrate (0.2 mg/kg IV). Approximately 30 minutes after premedication, anesthesia was induced with propofol (2.6-6.6 mg/kg IV) and the dogs were intubated. General anesthesia was maintained via isoflurane (1-3% with 100% oxygen at approximately 1 L/min). Mechanical ventilation was performed as needed. Following the MR examination, all dogs were recovered and returned to animal housing for transfer to another non-terminal project.

**MRI**

All examinations were performed on a twin-gradient 3.0 T Signa HDx GE MR unit, using a single-channel knee coil. The dogs were in a prone position and the brain was centered in the coil. The head was restrained with tape and sponges to ensure no alteration in skull position within the coil during the course of the MRI examination.

The imaging protocol was initiated with one or more 3-plane localizer sequences, which were used to ensure uniform signal intensity across the skull, straight positioning within the coil and to plan T2-weighted (T2w) fast spin echo (FSE) transverse images. For T2w images, echo time (TE) was 30 msec, repetition time (TR) was 3000 msec, and an 18 cm field of view (FOV) and phase and frequency matrix of 356 x 224 were used. For this MR unit, spectroscopy planning requires that the transverse image plane is not altered (i.e. oblique in any plane) from its alignment with x-plane relative to $B_0$, representing the z-plane. The transverse T2w images were also used to confirm brain parenchymal normalcy, which was determined by a board certified radiologist (SPH) and neurologist (SRP).

**$^1$H-MRS**

Two-dimensional multi-voxel point resolved spectroscopy (PRESS) chemical shift imaging (CSI) was performed to obtain $^1$H-MRS brain spectra. This was done with water suppression and automatic shimming. The line width was

maintained below 13 Hz; this is a standard for canine brain $^{1}$H-MRS at our institution and most consistently results in diagnostic spectra. The echo time (TE) was set at 144 msec, repetition time (TR) at 1500 msec, and phase and frequency matrix at 8 x 8. The field of view (FOV), slice thickness and NEX were variable, depending on the voxel size. Intermediate TEs have reduced signal intensity relative to short TEs and thus are ideal to complete determination of nominal obtainable voxel size in the canine brain. Three regions of the brain were examined, which included the thalamus (Thal), piriform lobe (Pirif) and the cerebellar medulla (CereMed). This was done while ensuring that the entirety of the voxel was centered within the tissue of interest. The software of the unit used displays the spectra on the center slice of the volume of tissue sample. To minimize and/or detect voxel contamination by neighboring neural tissue types as well as to determine exact positioning of the voxel, the most rostral and caudal slices within the voxels were saved (See Figures 2a-c).

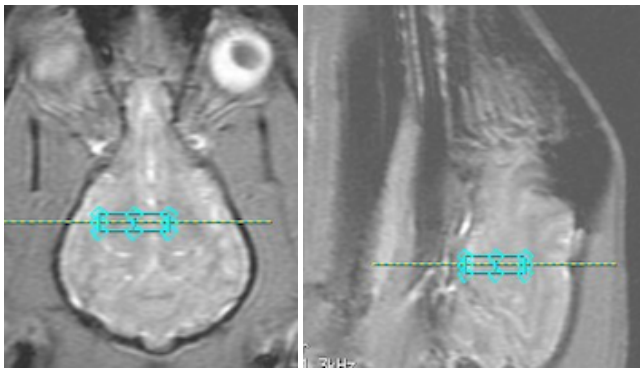

Figure 2 (a): 0.5 $cm^3$ Thalamus localizer

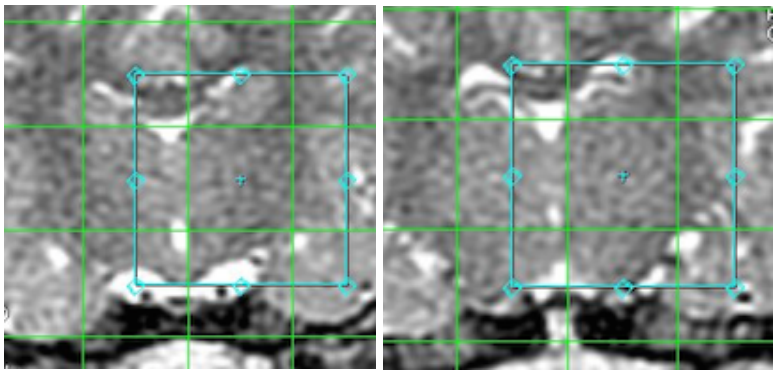

Figure 2 (b and c): 0.5 $cm^3$ Thalamus voxel first and last slice. First slice is on the left. Last slice is on the right. The blue box is the region of interest (ROI) and contains the center voxel with a blue cross. The green lines represent the matrix. The FOV is not shown.

Nominal voxel determination was evaluated in the Thal, using the following voxel sizes: 0.5, 0.4, 0.306 and 0.225 $cm^3$. The largest voxel was established by a pilot study of thalamic volume measurement from normal canine clinical brain MRIs. Voxels over 0.5 $cm^3$, which includes those previously researched in the canine brain (Martin-Vaquero *et.al.* 2012, Ober *et.al.* 2013, Warrington *et.al.* 2013), include adjacent neuroanatomical tissues in most canine brains. To accomplish these discrete voxels size, the following chart was used to determine

the slice thickness and phase and frequency matrix needed (Table 5). It is noteworthy that the white area on the chart represents the recommended voxel sizes by GE (General Electric Company, Fairfield CT). Table 6 below provides information on how the voxel sizes were obtained in the thalamus.

Table 5: GE Guidelines for acquiring certain voxel sizes

| | | | Probe P Guidelines to Follow | | | | | | | | |
|---|---|---|---|---|---|---|---|---|---|---|---|
| | | | stay above .5 on voxel | | | | | | | | |
| | *Freq or Phase* | Voxel Thickness | | | | | | | | | |
| FOV | 8 | 0.1 | 0.2 | 0.3 | 0.4 | 0.5 | 0.6 | 0.7 | 0.8 | 0.9 | 1 |
| 8 | 1.00 | 0.1 | 0.2 | 0.3 | 0.4 | 0.5 | 0.6 | 0.7 | 0.8 | 0.9 | 1 |
| 9 | 1.13 | 0.12656 | 0.25313 | 0.37969 | 0.50625 | 0.63281 | 0.75938 | 0.88594 | 1.0125 | 1.13906 | 1.265625 |
| 10 | 1.25 | 0.15625 | 0.3125 | 0.46875 | 0.625 | 0.78125 | 0.9375 | 1.09375 | 1.25 | 1.40625 | 1.5625 |
| 11 | 1.38 | 0.18906 | 0.37813 | 0.56719 | 0.75625 | 0.94531 | 1.13438 | 1.32344 | 1.5125 | 1.70156 | 1.890625 |
| 12 | 1.50 | 0.225 | 0.45 | 0.675 | 0.9 | 1.125 | 1.35 | 1.575 | 1.8 | 2.025 | 2.25 |
| 13 | 1.63 | 0.26406 | 0.52813 | 0.79219 | 1.05625 | 1.32031 | 1.58438 | 1.84844 | 2.1125 | 2.37656 | 2.640625 |
| 14 | 1.75 | 0.30625 | 0.6125 | 0.91875 | 1.225 | 1.53125 | 1.8375 | 2.14375 | 2.45 | 2.75625 | 3.0625 |
| 15 | 1.88 | 0.35156 | 0.70313 | 1.05469 | 1.40625 | 1.75781 | 2.10938 | 2.46094 | 2.8125 | 3.16406 | 3.515625 |
| 16 | 2.00 | 0.4 | 0.8 | 1.2 | 1.6 | 2 | 2.4 | 2.8 | 3.2 | 3.6 | 4 |
| 17 | 2.13 | 0.45156 | 0.90313 | 1.35469 | 1.80625 | 2.25781 | 2.70938 | 3.16094 | 3.6125 | 4.06406 | 4.515625 |
| 18 | 2.25 | 0.50625 | 1.0125 | 1.51875 | 2.025 | 2.53125 | 3.0375 | 3.54375 | 4.05 | 4.55625 | 5.0625 |
| 19 | 2.38 | 0.56406 | 1.12813 | 1.69219 | 2.25625 | 2.82031 | 3.38438 | 3.94844 | 4.5125 | 5.07656 | 5.640625 |
| 20 | 2.50 | 0.625 | 1.25 | 1.875 | 2.5 | 3.125 | 3.75 | 4.375 | 5 | 5.625 | 6.25 |
| 21 | 2.63 | 0.68906 | 1.37813 | 2.06719 | 2.75625 | 3.44531 | 4.13438 | 4.82344 | 5.5125 | 6.20156 | 6.890625 |
| 22 | 2.75 | 0.75625 | 1.5125 | 2.26875 | 3.025 | 3.78125 | 4.5375 | 5.29375 | 6.05 | 6.80625 | 7.5625 |
| 23 | 2.88 | 0.82656 | 1.65313 | 2.47969 | 3.30625 | 4.13281 | 4.95938 | 5.78594 | 6.6125 | 7.43906 | 8.265625 |
| 24 | 3.00 | 0.9 | 1.8 | 2.7 | 3.6 | 4.5 | 5.4 | 6.3 | 7.2 | 8.1 | 9 |

The NEX value was adjusted to maintain the relative SNR as voxel size decreased. The NEX values were not increased beyond a scan time that was considered clinically feasible. Scan times are calculated by the TR (which was maintained at 1500 ms), multiplied by the number of phase-encoding steps, multiplied by the NEX. With a 2D sequence, such as the ones used in the study,

there are two phase-encoding directions. As mentioned, the frequency and phase encoding matrix was maintained at 8 x 8 for all studies. Therefore, for the 0.5 $cm^3$ voxels at 1 NEX, the scan time is calculated as follows: Scan time = 1.5 s x 8 x 8 x 1 = 96 sec (1 minute and 36 seconds). For 0.5 $cm^3$ and 0.4$cm^3$ at 2 NEX the scan time was 3 minutes and 18 seconds. For 0.306 $cm^3$ at 4 NEX, 6 minutes and 30 seconds. For the 0.225 $cm^3$ voxels at 6 NEX, the scan time was 9 minutes and 43 seconds.

Table 6: MRI parameters changed to obtain various small voxel sizes. The FOV, phase and frequency matrix and slice thickness used in these dogs determine Thal voxel size. The NEX was increased as voxel size decreased in order to maintain sufficient signal to noise ratio (SNR).

| Voxel size ($cm^3$) | Slice Thickness (mm) | Matrix (phase x frequency) | Field of View (FOV) (cm) | Number of averages (NEX) |
|---|---|---|---|---|
| 0.5 | 5 | 8 x 8 | 8 | 1 or 2 |
| 0.4 | 4 | 8 x 8 | 8 | 2 |
| 0.306 | 4 | 8 x 8 | 7 | 4 |
| 0.225 | 4 | 8 x 8 | 6 | 6 |

The 0.225 $cm^3$ voxels were also tested in the piriform lobe (Pirif) and cerebellar medulla (CereMed). Care was taken to avoid placement of the voxel of interest in areas contaminated with water (i.e. CSF) and lipid (i.e. calvarium).

The post-processing software provided on the MR unit was used to produce the spectra for all dogs. The data was also evaluated offline using LCModel. Each voxel was evaluated for the following metabolites and metabolite

ratios: NAA, Cho, Cr, NAA/Cr, Cho/Cr and NAA/Cho. The metabolite concentrations were recorded and grouped by voxel size for further evaluation. SNR was estimated by determining the percent baseline noise for each spectrum. This was performed by determining the range of baseline noise (in MR Units) and dividing this range by the overall MR Unit range of each spectrum.

## STATISTICAL ANALYSIS

Means and standard deviation for the major metabolites (NAA, Cho and Cr) and metabolite ratios (NAA/Cr, NAA/Cho, Cho/Cr) were calculated, as well as the percent baseline noise. Two-way ANOVA procedures were performed to test the effects of voxel volume and the effects of the dogs. The least squared means of voxel volume were separated using a Tukey-Kramer procedure. A Shapiro-Wilk test was performed as an analysis of normal distribution. All of the metabolites and metabolite ratios were normally distributed. A logarithmic transformation was performed for percent baseline noise in order to normalize these observations. Some spectra from 4/8 dogs were not saved correctly and could not be included for statistical analysis. The significance level was set at 0.05 for all procedures.

Title: RESULTS

The descriptive analysis for the major metabolite concentrations (MR Units) and metabolite ratios are given in Table 5. The standard deviations for the major metabolite concentrations (in MR Units) were quite large. This was less notable for metabolite ratios, which were similar to the values obtained previously.[124] We compared the major metabolite concentrations, metabolite ratios and percent baseline noise across 4 voxel volumes in the Thal.

The metabolites with statistically significant differences across voxel volumes were Cr and NAA. The mean Cr was significantly greater in the 0.3 $cm^3$ voxel volume when compared to the 0.5 $cm^3$ voxel ($p = 0.0210$). There is no significant difference in mean Cr between the other voxel volumes. For NAA, there are significant differences based on volume ($p = 0.0459$), but after adjusting for multiple comparisons, there was no statistically significant difference across voxel volumes. However, there was a clear trend for increasing mean NAA as voxel volume decreases. There is no statistically significant difference across voxel volumes for mean Cho ($p = 0.1546$). There is a trend, however, for the average Cho to be greater as voxel volume decreases.

The metabolite ratios with significant differences across voxel volumes were NAA/Cr and Cho/Cr. The mean NAA/Cr was significantly greater for the

0.225 $cm^3$ voxel compared to all other volumes (p = 0.0019). There was no statistical difference in NAA/Cr between the 0.3, 0.4 and 0.5$cm^3$ voxel volumes. The mean Cho/Cr is statistically greater in the 0.225 $cm^3$ voxel compared to the 0.5 $cm^3$ voxel (p = 0.0422). The measures do not go in any order for voxel volumes. The other volumes are not statistically different for Cho/Cr. There were no statistically significant differences across volumes for NAA/Cho (p = 0.5629).

There was a statistically significant dog effect across all volumes for each variable. The mean ln (percent baseline noise) was significantly larger for the 0.5 $cm^3$ voxel volume compared to both the 0.306 $cm^3$ and 0.225 $cm^3$ voxel volumes (p = 0.0023), but not statistically different from the 0.4$cm^3$ voxel.

Table 7. $^{1}$H-MRS metabolite concentrations and ratios from normal dogs. The mean and standard deviation of the nominal peak height for multiple brain metabolites (NAA, Cho and Cr) and metabolite ratios (NAA/Cho, NAA/Cr and Cho/Cr) from MRSI $^{1}$H-MRS of three brain regions various voxel sizes and NEX. Values with an asterisk were of statistical significant. Significance level was set at 0.05.

| Voxel volume ($cm^3$) | NAA | Cho | Cr | NAA/Cr | NAA/Cho | Cho/Cr |
|---|---|---|---|---|---|---|
| Thal 0.5 (1NEX) | 4515 ± 3259 | 5069± 3412 | 3881± 2027 * | 1.127± 0.328 * | 0.933± 0.233 | 1.289± 0.503 * |
| Thal 0.5 (2NEX) | 6365± 5.622 | 5935 ± 4961 | 5159 ± 2564 * | 1.087 ± 0.559 * | 1.170 ± 0.736 | 1.035 ± 0.454 * |
| Thal 0.4 | 5620± 4294 | 5697± 4508 | 4736± 2341 | 1.037± 0.413 * | 0.987± 0.173 | 1.022± 0.441 |
| Thal 0.306 | 15801± 5945 | 6388± 5205 | 6155± 2815 * | 1.069± 0.551 * | 1.214± 0.607 | 0.935± 0.429 |
| Thal 0.225 | 8075± 5812 | 7518± 6470 | 4523± 3069 | 1.712± 0.303 * | 1.282± 0.041 | 1.448± 0.500 * |
| Pirif 0.225 | 9440± 5574 | 7016± 3337 | 5594± 3459 | 1.99± 1.07 | 1.329± 0.47 | 1.55± 0.843 |
| CereMed 0.225 | 7452± 3449 | 6838± 3740 | 6754± 3448 | 1.245± 0.494 | 1.362± 0.840 | 0.973± 0.195 |

Though voxel contamination was minimal, compared with prior $^{1}$H-MRS studies of the canine brain, there was some contribution of adjacent tissue types to the center voxel spectra, particularly when using the larger voxel sizes. Figure 4 exemplifies this contamination.

For the Thal 0.5 $cm^3$, 0.4 $cm^3$ and 0.306 $cm^3$ voxels, there is some contamination by the adjacent internal capsule white matter in 7/8 dogs. In 3/8

dogs, the 0.5 $cm^3$ Thal voxel extends into the area of the basal nucleus. The Pirif voxels had mild voxel contamination by the adjacent internal capsule white matter (3/7 dogs). The CereMed voxels, though centered in the white matter of the cerebellar medulla and arbor vitae, had some contribution by the folia of gray matter in all dogs.

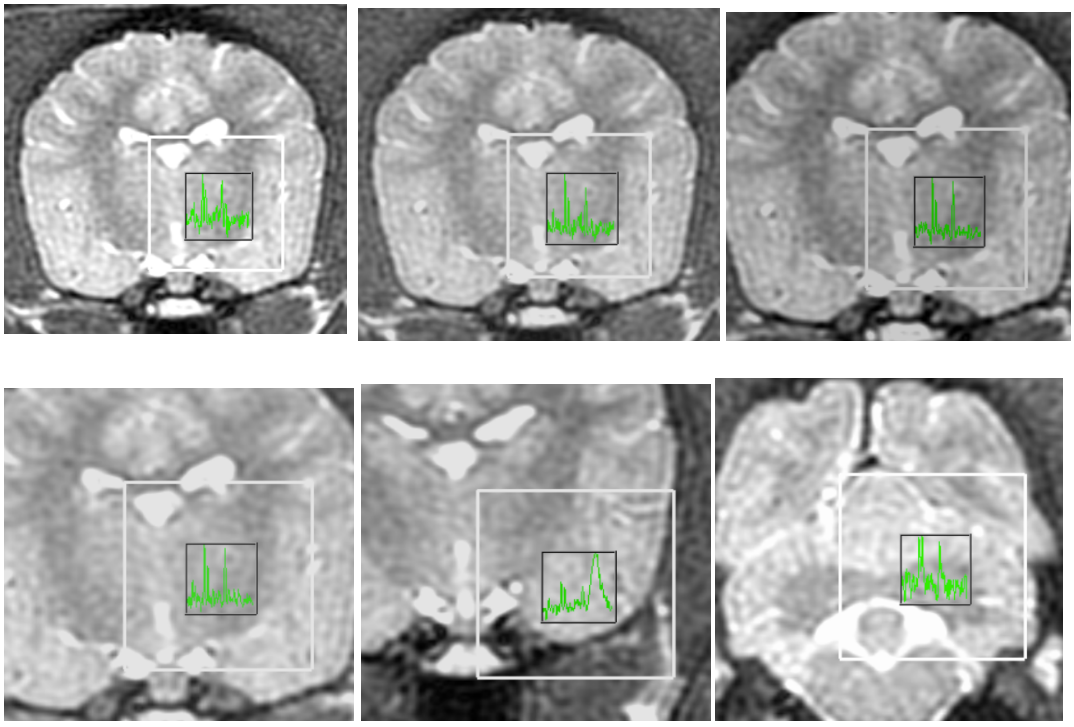

Figure 3 (a-f): Demonstration of mild voxel contamination. Top row, from left to right; 0.5 $cm^3$, 0.4$cm^3$ and 0.306 $cm^3$ voxels in the thalamus. Bottom row from left to right; 0.225 $cm^3$ voxels in the Thal, Pirif and CereMed. The white box represents the volume of interest (ROI). The black box represents the center voxel. FOV and matrix are not shown.

There is extension of the ROI outside of the calvarium in both the Pirif and CereMed sequences. Ober *et al.* (2013) discussed poorer quality MRSI spectra when the ROI was placed with the edges outside of the brain parenchyma. This was thought to be due to prominent lipid peaks, despite the use of saturation bands.[123] A large visible lipid peak was present on many Pirif spectra from our study (5/7 dogs). Additionally, the VOI, and to a lesser extent, the center voxel, extend over CSF of the subarachnoid spaces and ventricles in the Pirf and CereMed scans. See Figure 4 below for examples of spectra from three different brain regions.

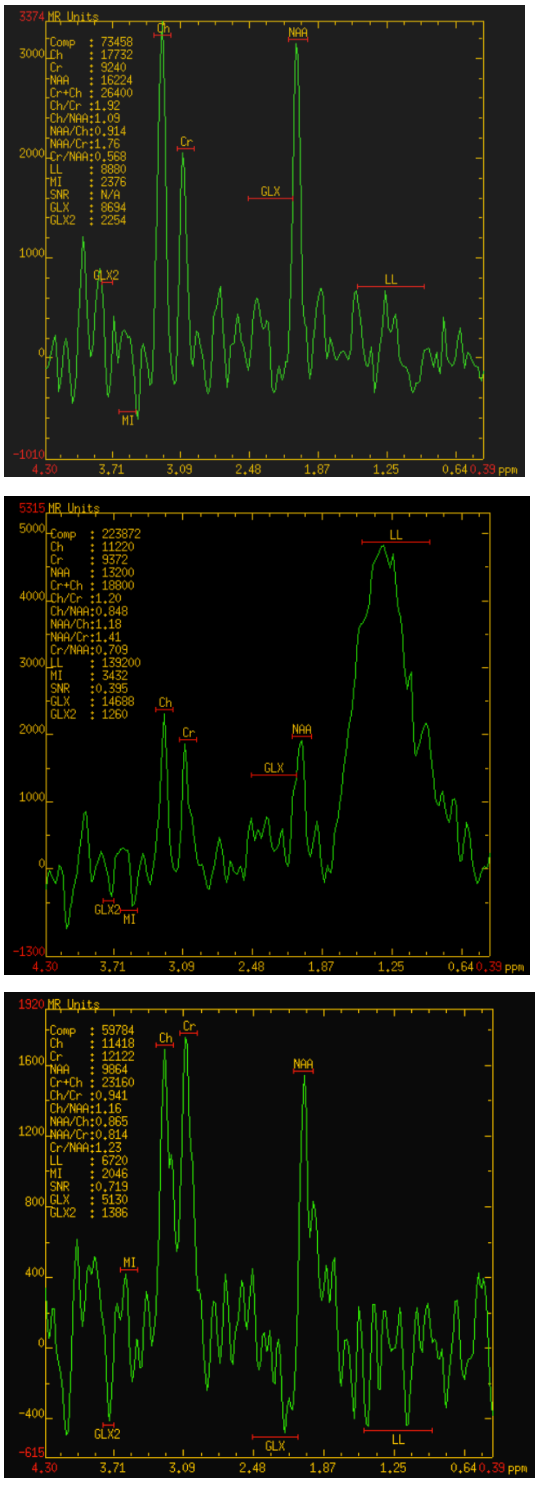


Figure 4 (a-c): 0.225 $cm^3$ voxel spectra from three brain regions of one dog. From top to bottom: Thal, Pirif and CereMed. Major metabolites NAA, Cho and Cr are identified at 2.01, 3.20 and 3.03 ppm respectively. A lipid peak at 0.9 and 1.5 ppm in present in some Pirif spectra.

There was significantly greater percent baseline noise in the 0.5 $cm^3$ voxel compared to the smaller voxel sizes (0.306 and 0.225 $cm^3$). The Thal ROIs also contained CSF of the lateral and third ventricles and subarachnoid spaces. Some of the Thal voxels had a large amount of visible baseline noise, to the point that the major metabolites (NAA, Cho and Cr) were obscured and appeared to be negatively reflected. See Figure 5 for an example of a Thal scan with significant baseline noise.

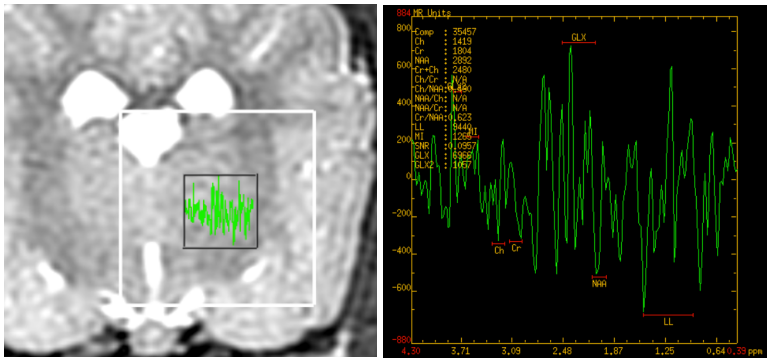


Figure 5: 0.225 $cm^3$ Thal voxel with appreciable baseline noise.

The $^1$H-MRS peaks from NAA, Cho and Cr were identifiable in 36/49, 39/49 and 43/49 spectra respectively. The mI and Glx peaks were more variable and were identified in 12/49 and 11/49 spectra respectively. The Lac peak was not identified in any spectra, as expected from normal dogs. A lipid peak was present in 5/7 Pirif spectra.

Title: CONCLUSIONS

Single voxel and multi-voxel $^{1}$H-MRS is a commonly employed and clinically useful imaging tool for non-invasive, neurochemical analysis. It has become widely used for the diagnosis, prognostication and monitoring of numerous human brain diseases, including neoplasia, infectious and inflammatory diseases, and ischemic and traumatic brain injury.[1] As a non-invasive, highly sensitive diagnostic test of brain diseases, $^{1}$H-MRS has the potential to be extremely clinically useful in veterinary medicine, since brain biopsy is a less commonly employed diagnostic tool when compared to human medicine. The original studies of animal brain $^{1}$H-MRS were performed as models for human disease.[49,79,119,120,129] Only in the past several years have researchers been interested in developing standardized protocols for $^{1}$H-MRS for use in clinical veterinary medicine.[121-125] Based on the techniques and findings in these recent studies, it is unclear if precise brain metabolite quantification can be performed in veterinary patients without voxel contamination by neighboring tissues.

Recent studies have reported reliable $^{1}$H-MRS evaluation of normal canine brain using 1.5 and 3 Tesla magnetic field strengths using both single voxel and multiple voxel techniques.[122-124] The purity of the samples is questionable based on descriptions of size and location of voxel placement. For instance, Martin-Vaquero *et al.* (2012) describes using a PRESS single-voxel technique with 1

$cm^3$ and 8 $cm^3$ volumes acquired from the parietal and cortical-ventricular areas of laboratory beagles.[122] While it may be possible to obtain sufficient signal for $^1$H-MRS, the likelihood of voxel contamination is high. Considering the small size of the canine brain, these are relatively large voxel sizes, especially 8 $cm^3$. As previously mentioned, based on a pilot study of normal brain MRI thalamic volume measurements, we determined that for most canine brains a 0.5 $cm^3$ voxel is the largest nominal voxel size that can be used without significant voxel contamination by adjacent tissues. Regardless of voxel size, the voxels placed in the cortical-ventricular area are contaminated by various tissue types by definition.

Warrington *et al.* (2013) reported the MRS metabolite concentrations and ratios of specific brain regions for normal beagles.[124] This study used 1.23 $cm^3$ voxels. The FOV for the voxels were centered on 6 different brain regions: the olfactory lobes, rostral edge of the corpus callosum, the interthalamic adhesion, rostral edge of cerebellum, centered in the cerebellum and centered in the brainstem.[124] It was reported that the individual voxels were placed entirely within brain parenchyma, however, there is great variability in the number of tissue types represented within each voxel. For instance, the voxels centered on the interthalamic adhesion contain gray matter, white matter and areas of the lateral and third ventricles.

As discussed by Ober *et al.* (2013), for a given field of view, a larger phase and frequency encoding matrix will create smaller voxel sizes and thus

improved spatial resolution.[123] This is especially important for $^{1}$H-MRS in the canine brain in order to resolve individual metabolite peaks in small volumes of tissue. Using canine cadavers, they determined that subjectively optimal MR spectra were acquired using a phase and frequency encoding matrix of 18 cm x 18 cm, with a slice thickness of 1 cm, for a resultant voxel volume of 1.23 cm$^{3}$.[123] In this study, however, voxels were centered on the thalamus in order to optimize the amount of brain parenchyma included within the voxels.[123] Therefore, this protocol may only be useful when larger regions of brain parenchyma or a lesion are being evaluated. When smaller regions need to be examined, such as lesions at the edge of brain parenchyma, a small voxel $^{1}$H-MRS technique should be used to minimize voxel contamination with adjacent structures and improve the specificity of the spectrum.

In our current study, we used 0.5, 0.4, 0.306 and 0.225 cm$^{3}$ voxel volumes for canine multi-voxel $^{1}$H-MRS of the Thal and 0.225 cm$^{3}$ voxels for two other brain regions (Pirif and CereMed). The former was performed to examine the effects of reducing VOI and determine if spectra could be produced within a reasonable time frame so that the sequence could be included in a routine MRI study. For each voxel volume, the resultant spectra from the Thal scans contained identifiable peaks of the major brain metabolites of interest (NAA, Cho and Cr). This indicates that this technique may be useful for small voxel canine $^{1}$H-MRS at 3.0 T. With the technique established, one could select the

appropriate VOI for a lesion of interest and predict the necessary time to achieve acceptable signal to produce spectra.

When the smallest voxel volume (0.225 $cm^3$) was centered in the Pirif and the CereMed, NAA, Cho and Cr were relatively identifiable in most spectra. This indicates that small voxel canine $^1$H-MRSI may be possible at 3.0 T to identify NAA, Cho and Cr in the Pirif and CereMed. The large lipid peak in the Pirif spectra may be secondary to extension of the ROI outside of the brain. The increased percentage baseline noise in the 0.5 $cm^3$ voxels compared to other voxel volumes may be associated with contamination by adjacent tissues. Though water suppression techniques are used with PRESS, CSF may be contributory to the spectra in these larger voxel volumes.

Other considerations for decreased spectral quality include inadequate lipid and water saturation techniques, insufficient high order shimming and less robust crusher gradients, which may all contribute to field inhomogeneity.[1] The type of coil used may also contribute to overall decreased SNR. Ober *et al* (2013) compared spectral quality of 3 different coils. There was subjectively improved spectral quality when using the quadrature extremity coil when comparison to an 8-channel head coil and neurovascular array coil. It is correct to presume that this was predominantly due to the smaller size of the extremity coil, which causes the anatomy of interest to be in closer proximity to the coil. However, no statistical significant difference was reached between coil types in this study.[123] The use of

phased array coils and multiple receiver channel MRI systems can be used to increase SNR and decrease scan time.[1]

Voxel specificity was one of our major goals in validating the use of small voxels for canine brain $^{1}$H-MRS. Although our spectra contained identifiable major metabolites, there was some amount of voxel contamination noted on most scans, except for the 0.225 $cm^3$ voxels centered on the Thal. In comparison to previous studies, the levels of voxel contamination were greatly reduced. This was achieved first by limiting the maximal voxel size to 0.5 $cm^3$ and secondly by verifying the tissue type within the first and last transverse slices that were included in each voxel. The ability to obtain pure spectra from discrete tissue volumes in canine brains that completely lack tissue contamination (i.e Pirif and CereMed or small brain lesions) may not be possible. Because of the shape of these structures, their small size and the proximity to the skull make them difficult to isolate in square or rectangular shaped voxels. Future studies on certain brain diseases in dogs, such as tumors or inflammatory diseases, may be limited to larger lesions. Voxel contamination in small lesions may alter the sensitivity and specificity of 1H-MRS for certain brain diseases.

We chose to use an intermediate (144 ms) TE for every scan. An intermediate TE is advantageous in that it allows identification of the major metabolites (NAA, Cho and Cr). Longer TEs are used more commonly because these techniques are less susceptible to artifacts from insufficient water suppression and have a flatter baseline, thus making metabolite identification

easier.[15] Additionally, in certain disease states where Lac may be present (e.g. abscesses), the Lac peak will be inverted at 144 ms, which helps to differentiate it from the near-by lipid peak. The differentiation of these is important because lactate is a marker of anaerobic metabolism and may be present with certain diseases such as infarcts. Lipids indicate the presence of necrosis or adipose tissue.[1,13,17,18]

The advantage using a short TE (< 40ms) is that there is decreased signal decay, which allows metabolites with short relaxation times such as small concentrations of lipid and additional metabolite peaks, such as Glu, Gln and mI are also identified.[1,16,130] We would expect that the voxel sizes developed in this study could be used to investigate the detection of these secondary metabolites in canine brain $^{1}$H-MRS.

As voxel volume decreased, we increased the NEX in order to increase the SNR. This was done based on physical premise that SNR would be inherently lower with a smaller amount of tissue being sampled. Increased scan times were needed to acquire subjectively diagnostic spectra. We limited the extent of NEX increases to maintain scan times that were considered clinically reasonable by a board certified veterinary radiologist and two board certified neurologists. Our scan times ranged from 1 minute and 36 seconds to 9 minutes and 43 seconds, with time increasing for smaller voxels. These results indicate that small voxels were feasible in canine brain $^{1}$H-MRS, and the appropriately sized voxel could be selected for a particular tissue type or lesion size.

The length of time that a scan protocol takes is of utmost importance in veterinary patients. Virtually all patients are under general anesthesia for MRI, and therefore it is imperative that we can perform a scan protocol within a clinically appropriate amount of time. Patients undergoing brain $^{1}$H-MRS will first have routine MRI scans that include at minimum T2w, T1-weighted (T1w) and post-contrast T1w sequences in multiple scan planes. The study would ideally be performed within 60 minutes at 1.5 T and less at 3.0 T. The addition of other sequences, such as diffusion weighted imaging or spectroscopy will lengthen the time the patient is in the MR scanner. However, the benefit of a non-invasive and specific diagnosis of intracranial disease could be a judicious use of additional time for determination of treatment options and prognostication.

We documented that small voxels for $^{1}$H-MRS were achievable in the canine brain. The challenge will be to acquire a sufficient number of known specific diseases to define the unique and distinguishing spectra appearance. It is tempting to extrapolate from human $^{1}$H-MRS, but there are known differences in canine and human tumor genotypes and phenotypes. Gliomas would be the best example of this and is a tumor type that has been extensively tested using $^{1}$H-MRS in humans.[1]

Title: REFERENCES


1. Barker PB, Bizzi A, Stefano ND, et al. Clinical MR spectroscopy: techniques and applications. Cambridge: Cambridge University Press, 2010.
2. van der Graaf M. In vivo magnetic resonance spectroscopy: basic methodology and clinical applications. *European Biophysics Journal: EBJ* 2010;39:527-540.
3. Hiremath GK, Najm IM. Magnetic resonance spectroscopy in animal models of epilepsy. *Epilepsia* 2007;48 Suppl 4:47-55.
4. Westbrook C, Roth CK, Talbot J. *MRI in Practice*. Third ed: Blackwell Publishing, 2006.
5. Mason GF. Magnetic resonance spectroscopy for studies of neurotransmission in vivo. *Psychopharmacology Bulletin* 2003;37:26-40.
6. Curry T.S. DJE, Murry R.C. *Christensen's Physics of Diagnostic Radiology*. fourth ed. Malvern, PA: Lea & Febinger, 1990.
7. Bushberg J.T. SJA, Leidholdt E.M., Boone J.M. . *The Essential Physics of Medical Imaging*. First ed. Baltimore, Ma: Williams & Wilkins, 1994.
8. Drost DJ, Riddle WR, Clarke GD. Proton magnetic resonance spectroscopy in the brain: report of AAPM MR Task Group #9. *Med Phys* 2002;29:2177-2197.
9. Brown M.A. SRC. *MRI Basic Principles and Applications*. Fourth ed. Hoboken, NJ: Wiley-Blackwell, 2010.
10. McPhail MJW, Taylor-Robinson SD. The role of magnetic resonance imaging and spectroscopy in hepatic encephalopathy. *Metabolic Brain Disease* 2010;25:65-72.
11. Ross B, Bluml S. Magnetic resonance spectroscopy of the human brain. *The Anatomical Record* 2001;265:54-84.
12. Mandal PK. In vivo proton magnetic resonance spectroscopic signal processing for the absolute quantitation of brain metabolites. *Eur J Radiol* 2012;81:e653-664.
13. Kwock L. Localized MR spectroscopy: basic principles. *Neuroimaging Clinics Of North America* 1998;8:713-731.
14. Mekle R, Mlynarik V, Gambarota G, et al. MR spectroscopy of the human brain with enhanced signal intensity at ultrashort echo times on a clinical platform at 3T and 7T. *Magn Reson Med* 2009;61:1279-1285.
15. Simister RJ, Woermann FG, McLean MA, et al. A Short-echo-time Proton Magnetic Resonance Spectroscopic Imaging Study of Temporal Lobe Epilepsy. *Epilepsia* 2002;43:1021-1031.
16. Soares DP, Law M. Magnetic resonance spectroscopy of the brain: review of metabolites and clinical applications. *Clinical Radiology* 2009;64:12-21.

17. Castillo M, Kwock L, Scatliff J, et al. Proton MR spectroscopy in neoplastic and non-neoplastic brain disorders. *Magnetic Resonance Imaging Clinics Of North America* 1998;6:1-20.

18. Yamasaki F, Takaba J, Ohtaki M, et al. Detection and differentiation of lactate and lipids by single-voxel proton MR spectroscopy. *Neurosurgical Review* 2005;28:267-277.

19. Kaminogo M, Ishimaru H, Morikawa M, et al. Diagnostic potential of short echo time MR spectroscopy of gliomas with single-voxel and point-resolved spatially localised proton spectroscopy of brain. *Neuroradiology* 2001;43:353-363.

20. Castillo M, Kwock L, Mukherji SK. Clinical applications of proton MR spectroscopy. *AJNR Am J Neuroradiol* 1996;17:1-15.

21. Frahm J, Bruhn H, Gyngell ML, et al. Localized high-resolution proton NMR spectroscopy using stimulated echoes: initial applications to human brain in vivo. *Magnetic Resonance In Medicine: Official Journal Of The Society Of Magnetic Resonance In Medicine / Society Of Magnetic Resonance In Medicine* 1989;9:79-93.

22. Teresi LM. *A Practicing Radiologist Guide to MR Spectroscopy of the Brain*
: Xlibris, 2007.

23. Kim D-S, Garwood M. High-field magnetic resonance techniques for brain research. *Current Opinion In Neurobiology* 2003;13:612-619.

24. Tkac I, Oz G, Adriany G, et al. In vivo 1H NMR spectroscopy of the human brain at high magnetic fields: metabolite quantification at 4T vs. 7T. *Magn Reson Med* 2009;62:868-879.

25. Panigrahy A, Borzage M, Blüml S. Basic principles and concepts underlying recent advances in magnetic resonance imaging of the developing brain. *Seminars In Perinatology* 2010;34:3-19.

26. Baslow MH. Evidence supporting a role for N-acetyl-L-aspartate as a molecular water pump in myelinated neurons in the central nervous system. An analytical review. *Neurochemistry International* 2002;40:295-300.

27. Tkac I, Rao R, Georgieff MK, et al. Developmental and regional changes in the neurochemical profile of the rat brain determined by in vivo 1H NMR spectroscopy. *Magnetic Resonance In Medicine: Official Journal Of The Society Of Magnetic Resonance In Medicine / Society Of Magnetic Resonance In Medicine* 2003;50:24-32.

28. Baslow MH. Brain N-acetylaspartate as a molecular water pump and its role in the etiology of Canavan disease: a mechanistic explanation. *Journal Of Molecular Neuroscience: MN* 2003;21:185-190.

29. Pal D, Bhattacharyya A, Husain M, et al. In vivo proton MR spectroscopy evaluation of pyogenic brain abscesses: a report of 194 cases. *AJNR American Journal Of Neuroradiology* 2010;31:360-366.

30. Demir MK, Iplikcioglu AC, Dincer A, et al. Single voxel proton MR spectroscopy findings of typical and atypical intracranial meningiomas. *Eur J Radiol* 2006;60:48-55.

31. Kang B-T, Jang D-P, Lee J-H, et al. Detection of cerebral metabolites in a canine model of ischemic stroke using 1H magnetic resonance spectroscopy. *Research in Veterinary Science* 2009;87:300-306.

32. Sundgren PC, Nagesh V, Elias A, et al. Metabolic alterations: a biomarker for radiation-induced normal brain injury-an MR spectroscopy study. *Journal Of Magnetic Resonance Imaging: JMRI* 2009;29:291-297.

33. Ratai E-M, Pilkenton SJ, Greco JB, et al. In vivo proton magnetic resonance spectroscopy reveals region specific metabolic responses to SIV infection in the macaque brain. *BMC Neuroscience* 2009;10:63-63.

34. Wittsack HJ, Kugel H, Roth B, et al. Quantitative measurements with localized 1H MR spectroscopy in children with Canavan's disease. *J Magn Reson Imaging* 1996;6:889-893.

35. Surendran S, Matalon KM, Tyring SK, et al. Molecular basis of Canavan's disease: from human to mouse. *J Child Neurol* 2003;18:604-610.

36. Urenjak J, Williams SR, Gadian DG, et al. Proton nuclear magnetic resonance spectroscopy unambiguously identifies different neural cell types. *The Journal Of Neuroscience: The Official Journal Of The Society For Neuroscience* 1993;13:981-989.

37. Braissant O, B√©ard E, Torrent Cl, et al. Dissociation of AGAT, GAMT and SLC6A8 in CNS: relevance to creatine deficiency syndromes. *Neurobiology Of Disease* 2010;37:423-433.

38. Haga KK, Khor YP, Farrall A, et al. A systematic review of brain metabolite changes, measured with 1H magnetic resonance spectroscopy, in healthy aging. *Neurobiology Of Aging* 2009;30:353-363.

39. Jacobs MA, Horska A, van Zijl PC, et al. Quantitative proton MR spectroscopic imaging of normal human cerebellum and brain stem. *Magn Reson Med* 2001;46:699-705.

40. Widhalm G, Krssak M, Minchev G, et al. Value of 1H-magnetic resonance spectroscopy chemical shift imaging for detection of anaplastic foci in diffusely infiltrating gliomas with non-significant contrast-enhancement. *J Neurol Neurosurg Psychiatr* 2011;82:512-520.

41. Li BSY, Wang H, Gonen O. Metabolite ratios to assumed stable creatine level may confound the quantification of proton brain MR spectroscopy. *Magnetic Resonance Imaging* 2003;21:923-928.

42. Mader I, Roser W, Kappos L, et al. Serial proton MR spectroscopy of contrast-enhancing multiple sclerosis plaques: absolute metabolic values over 2 years during a clinical pharmacological study. *AJNR American Journal Of Neuroradiology* 2000;21:1220-1227.

43. Pan JW, Hetherington HP, Vaughan JT, et al. Evaluation of multiple sclerosis by 1H spectroscopic imaging at 4.1 T. *Magnetic Resonance In Medicine: Official Journal Of The Society Of Magnetic Resonance In Medicine / Society Of Magnetic Resonance In Medicine* 1996;36:72-77.

44. Allen IV, McKeown SR. A histological, histochemical and biochemical study of the macroscopically normal white matter in multiple sclerosis. *J Neurol Sci* 1979;41:81-91.

45. Gideon P, Henriksen O, Sperling B, et al. Early time course of N-acetylaspartate, creatine and phosphocreatine, and compounds containing choline

in the brain after acute stroke. A proton magnetic resonance spectroscopy study. *Stroke; A Journal Of Cerebral Circulation* 1992;23:1566-1572.

46. Peres M, Bourgeois D, Roussel S, et al. Two-dimensional 1H spectroscopic imaging for evaluating the local metabolic response to focal ischemia in the conscious rat. *NMR Biomed* 1992;5:11-19.

47. Strange K, Emma F, Paredes A, et al. Osmoregulatory changes in myo-inositol content and Na+/myo-inositol cotransport in rat cortical astrocytes. *Glia* 1994;12:35-43.

48. Wilken B, Dechent P, Herms J, et al. Quantitative proton magnetic resonance spectroscopy of focal brain lesions. *Pediatric Neurology* 2000;23:22-31.

49. Whelan HT, Clanton JA, Moore PM, et al. Magnetic resonance brain tumor imaging in canine glioma. *Neurology* 1987;37:1235-1239.

50. Verbruggen KT, Meiners LC, Sijens PE, et al. Magnetic resonance imaging and proton magnetic resonance spectroscopy of the brain in the diagnostic evaluation of developmental delay. *European Journal Of Paediatric Neurology: EJPN: Official Journal Of The European Paediatric Neurology Society* 2009;13:181-190.

51. McKnight TR, Noworolski SM, Vigneron DB, et al. An automated technique for the quantitative assessment of 3D-MRSI data from patients with glioma. *J Magn Reson Imaging* 2001;13:167-177.

52. Bruhn H, Michaelis T, Merboldt KD, et al. On the interpretation of proton NMR spectra from brain tumours in vivo and in vitro. *NMR In Biomedicine* 1992;5:253-258.

53. Horska A, Barker PB. Imaging of brain tumors: MR spectroscopy and metabolic imaging. *Neuroimaging Clin N Am* 2010;20:293-310.

54. Kaiser LG, Schuff N, Cashdollar N, et al. Age-related glutamate and glutamine concentration changes in normal human brain: 1H MR spectroscopy study at 4 T. *Neurobiology Of Aging* 2005;26:665-672.

55. Malhotra HS, Jain KK, Agarwal A, et al. Characterization of tumefactive demyelinating lesions using MR imaging and in-vivo proton MR spectroscopy. *Multiple Sclerosis (Houndmills, Basingstoke, England)* 2009;15:193-203.

56. Meldrum BS. Glutamate as a neurotransmitter in the brain: review of physiology and pathology. *J Nutr* 2000;130:1007S-1015S.

57. Kreis R, Ross BD, Farrow NA, et al. Metabolic disorders of the brain in chronic hepatic encephalopathy detected with H-1 MR spectroscopy. *Radiology* 1992;182:19-27.

58. Holshouser BA, Tong KA, Ashwal S. Proton MR spectroscopic imaging depicts diffuse axonal injury in children with traumatic brain injury. *AJNR Am J Neuroradiol* 2005;26:1276-1285.

59. Shutter L, Tong KA, Holshouser BA. Proton MRS in acute traumatic brain injury: role for glutamate/glutamine and choline for outcome prediction. *J Neurotrauma* 2004;21:1693-1705.

60. Macri MA, D'Alessandro N, Di Giulio C, et al. Region-specific effects on brain metabolites of hypoxia and hyperoxia overlaid on cerebral ischemia in young and old rats: a quantitative proton magnetic resonance spectroscopy study. *Journal Of Biomedical Science* 2010;17:14-14.

61. Sontheimer H. A role for glutamate in growth and invasion of primary brain tumors. *J Neurochem* 2008;105:287-295.
62. Jaskolski DJ, Fortuniak J, Majos A, et al. Magnetic resonance spectroscopy in intracranial tumours of glial origin. *Neurol Neurochir Pol* 2013;47:438-449.
63. Rothman DL, Petroff OA, Behar KL, et al. Localized 1H NMR measurements of gamma-aminobutyric acid in human brain in vivo. *Proc Natl Acad Sci U S A* 1993;90:5662-5666.
64. Puts NA, Edden RA. In vivo magnetic resonance spectroscopy of GABA: a methodological review. *Prog Nucl Magn Reson Spectrosc* 2012;60:29-41.
65. Levy LM, Degnan AJ. GABA-Based Evaluation of Neurologic Conditions: MR Spectroscopy. *AJNR Am J Neuroradiol* 2012.
66. Petroff OAC, Pleban LA, Spencer DD. Symbiosis between in vivo and in vitro NMR spectroscopy: The creatine, N-acetylaspartate, glutamate, and GABA content of the epileptic human brain. *Magnetic Resonance Imaging* 1995;13:1197-1211.
67. Kelley DAC, Wald LL, Star-Lack JM. Lactate detection at 3T: Compensating J coupling effects with BASING. *Journal of Magnetic Resonance Imaging* 1999;9:732-737.
68. Nagae-Poetscher LM, McMahon M, Braverman N, et al. Metabolites in ventricular cerebrospinal fluid detected by proton magnetic resonance spectroscopic imaging. *Journal of Magnetic Resonance Imaging* 2004;20:496-500.
69. Sappey-Marinier D, Calabrese G, Hetherington HP, et al. Proton magnetic resonance spectroscopy of human brain: applications to normal white matter, chronic infarction, and MRI white matter signal hyperintensities. *Magnetic Resonance In Medicine: Official Journal Of The Society Of Magnetic Resonance In Medicine / Society Of Magnetic Resonance In Medicine* 1992;26:313-327.
70. Brand A, Richter-Landsberg C, Leibfritz D. Multinuclear NMR studies on the energy metabolism of glial and neuronal cells. *Developmental Neuroscience* 1993;15:289-298.
71. Yue Q, Isobe T, Shibata Y, et al. New observations concerning the interpretation of magnetic resonance spectroscopy of meningioma. *Eur Radiol* 2008;18:2901-2911.
72. Cho YD, Choi GH, Lee SP, et al. (1)H-MRS metabolic patterns for distinguishing between meningiomas and other brain tumors. *Magn Reson Imaging* 2003;21:663-672.
73. Noworolski SM, Nelson SJ, Henry RG, et al. High spatial resolution 1H-MRSI and segmented MRI of cortical gray matter and subcortical white matter in three regions of the human brain. *Magn Reson Med* 1999;41:21-29.
74. Pfefferbaum A, Adalsteinsson E, Spielman D, et al. In vivo spectroscopic quantification of the N-acetyl moiety, creatine, and choline from large volumes of brain gray and white matter: effects of normal aging. *Magn Reson Med* 1999;41:276-284.
75. Kreis R, Ernst T, Ross BD. Development of the human brain: in vivo quantification of metabolite and water content with proton magnetic resonance spectroscopy. *Magnetic Resonance In Medicine: Official Journal Of The Society Of*

*Magnetic Resonance In Medicine / Society Of Magnetic Resonance In Medicine* 1993;30:424-437.

76. Michaelis T, Merboldt KD, Bruhn H, et al. Absolute concentrations of metabolites in the adult human brain in vivo: quantification of localized proton MR spectra. *Radiology* 1993;187:219-227.

77. Pouwels PJ, Frahm J. Regional metabolite concentrations in human brain as determined by quantitative localized proton MRS. *Magnetic Resonance In Medicine: Official Journal Of The Society Of Magnetic Resonance In Medicine / Society Of Magnetic Resonance In Medicine* 1998;39:53-60.

78. Wiebenga OT, Klauser AM, Nagtegaal GJ, et al. Longitudinal absolute metabolite quantification of white and gray matter regions in healthy controls using proton MR spectroscopic imaging. *NMR Biomed* 2014;27:304-311.

79. Anderson JH, Strandberg JD, Wong DF, et al. Multimodality correlative study of canine brain tumors. Proton magnetic resonance spectroscopy, positron emission tomography, and histology. *Investigative Radiology* 1994;29:597-605.

80. Bendini M, Marton E, Feletti A, et al. Primary and metastatic intraaxial brain tumors: prospective comparison of multivoxel 2D chemical-shift imaging (CSI) proton MR spectroscopy, perfusion MRI, and histopathological findings in a group of 159 patients. *Acta Neurochir (Wien)* 2011;153:403-412.

81. Buhl R, Stark AM, Hugo HH, et al. Gliosarcoma: clinical experiences and additional information with MR spectroscopy. *Neurological Research* 2009;31:873-877.

82. Fountas KN, Kapsalaki EZ, Gotsis SD, et al. In vivo proton magnetic resonance spectroscopy of brain tumors. *Stereotactic And Functional Neurosurgery* 2000;74:83-94.

83. Gillies RJ, Bhujwalla ZM, Evelhoch J, et al. Applications of magnetic resonance in model systems: tumor biology and physiology. *Neoplasia (New York, NY)* 2000;2:139-151.

84. Gillies RJ, Raghunand N, Karczmar GS, et al. MRI of the tumor microenvironment. *Journal Of Magnetic Resonance Imaging: JMRI* 2002;16:430-450.

85. Hourani R, Horska A, Albayram S, et al. Proton magnetic resonance spectroscopic imaging to differentiate between nonneoplastic lesions and brain tumors in children. *J Magn Reson Imaging* 2006;23:99-107.

86. Kinoshita Y, Yokota A. Absolute concentrations of metabolites in human brain tumors using in vitro proton magnetic resonance spectroscopy. *NMR In Biomedicine* 1997;10:2-12.

87. Lehnhardt FG, R√ ∂ hn G, Ernestus RI, et al. 1H- and (31)P-MR spectroscopy of primary and recurrent human brain tumors in vitro: malignancy-characteristic profiles of water soluble and lipophilic spectral components. *NMR In Biomedicine* 2001;14:307-317.

88. Meyerand ME, Pipas JM, Mamourian A, et al. Classification of biopsy-confirmed brain tumors using single-voxel MR spectroscopy. *AJNR American Journal Of Neuroradiology* 1999;20:117-123.

89. Stadlbauer A, Gruber S, Nimsky C, et al. Preoperative grading of gliomas by using metabolite quantification with high-spatial-resolution proton MR spectroscopic imaging. *Radiology* 2006;238:958-969.

90. Terpstra M, High WB, Luo Y, et al. Relationships among lactate concentration, blood flow and histopathologic profiles in rat C6 glioma. *NMR In Biomedicine* 1996;9:185-194.

91. Tong Z, Yamaki T, Harada K, et al. In vivo quantification of the metabolites in normal brain and brain tumors by proton MR spectroscopy using water as an internal standard. *Magnetic Resonance Imaging* 2004;22:735-742.

92. Zonari P, Baraldi P, Crisi G. Multimodal MRI in the characterization of glial neoplasms: the combined role of single-voxel MR spectroscopy, diffusion imaging and echo-planar perfusion imaging. *Neuroradiology* 2007;49:795-803.

93. Kounelakis MG, Zervakis ME, Postma GJ, et al. Revealing the metabolic profile of brain tumors for diagnosis purposes. *Conf Proc IEEE Eng Med Biol Soc* 2009;2009:35-38.

94. Vuori K, Kankaanranta L, Hakkinen AM, et al. Low-grade gliomas and focal cortical developmental malformations: differentiation with proton MR spectroscopy. *Radiology* 2004;230:703-708.

95. McKnight TR, von dem Bussche MH, Vigneron DB, et al. Histopathological validation of a three-dimensional magnetic resonance spectroscopy index as a predictor of tumor presence. *J Neurosurg* 2002;97:794-802.

96. Hoehn M, Nicolay K, Franke C, et al. Application of magnetic resonance to animal models of cerebral ischemia. *Journal Of Magnetic Resonance Imaging: JMRI* 2001;14:491-509.

97. Franke C, Brinker G, Pillekamp F, et al. Probability of metabolic tissue recovery after thrombolytic treatment of experimental stroke: a magnetic resonance spectroscopic imaging study in rat brain. *J Cereb Blood Flow Metab* 2000;20:583-591.

98. Rumpel H, Khoo JB, Chang HM, et al. Correlation of the apparent diffusion coefficient and the creatine level in early ischemic stroke: a comparison of different patterns by magnetic resonance. *Journal Of Magnetic Resonance Imaging: JMRI* 2001;13:335-343.

99. Graham GD, Blamire AM, Rothman DL, et al. Early temporal variation of cerebral metabolites after human stroke. A proton magnetic resonance spectroscopy study. *Stroke; A Journal Of Cerebral Circulation* 1993;24:1891-1896.

100. Parsons MW, Li T, Barber PA, et al. Combined (1)H MR spectroscopy and diffusion-weighted MRI improves the prediction of stroke outcome. *Neurology* 2000;55:498-505.

101. Mader I, Rauer S, Gall P, et al. 1H MR spectroscopy of inflammation, infection and ischemia of the brain. *European Journal of Radiology* 2008;67:250-257.

102. Dimou S, Lagopoulos J. Towards objective markers of concussion in sport: a review of white matter and neurometabolic changes in the brain following sports-related concussion. *J Neurotrauma* 2013.

103. Garnett MR, Blamire AM, Rajagopalan B, et al. Evidence for cellular damage in normal-appearing white matter correlates with injury severity in patients following traumatic brain injury: A magnetic resonance spectroscopy study. *Brain* 2000;123 ( Pt 7):1403-1409.

104. Ashwal S, Holshouser BA, Shu SK, et al. Predictive value of proton magnetic resonance spectroscopy in pediatric closed head injury. *Pediatr Neurol* 2000;23:114-125.

105. Ross BD, Ernst T, Kreis R, et al. 1H MRS in acute traumatic brain injury. *J Magn Reson Imaging* 1998;8:829-840.

106. Aaen GS, Holshouser BA, Sheridan C, et al. Magnetic resonance spectroscopy predicts outcomes for children with nonaccidental trauma. *Pediatrics* 2010;125:295-303.

107. Cecil KM, Hills EC, Sandel ME, et al. Proton magnetic resonance spectroscopy for detection of axonal injury in the splenium of the corpus callosum of brain-injured patients. *Journal Of Neurosurgery* 1998;88:795-801.

108. Brooks WM, Friedman SD, Gasparovic C. Magnetic resonance spectroscopy in traumatic brain injury. *The Journal Of Head Trauma Rehabilitation* 2001;16:149-164.

109. Ashwal S, Holshouser B, Tong K, et al. Proton MR spectroscopy detected glutamate/glutamine is increased in children with traumatic brain injury. *J Neurotrauma* 2004;21:1539-1552.

110. Ashwal S, Holshouser B, Tong K, et al. Proton spectroscopy detected myoinositol in children with traumatic brain injury. *Pediatr Res* 2004;56:630-638.

111. Brant-Zawadzki M, Enzmann DR, Placone RC, Jr., et al. NMR imaging of experimental brain abscess: comparison with CT. *AJNR American Journal Of Neuroradiology* 1983;4:250-253.

112. Garg M, Gupta RK, Husain M, et al. Brain abscesses: etiologic categorization with in vivo proton MR spectroscopy. *Radiology* 2004;230:519-527.

113. Luthra G, Parihar A, Nath K, et al. Comparative evaluation of fungal, tubercular, and pyogenic brain abscesses with conventional and diffusion MR imaging and proton MR spectroscopy. *AJNR, American Journal of Neuroradiology*. Oak Brook; USA: American Society of Neuroradiology, 2007;1332-1338.

114. Gonzalez-Toledo E, Kelley RE, Minagar A. Role of magnetic resonance spectroscopy in diagnosis and management of multiple sclerosis. *Neurological Research* 2006;28:280-283.

115. Roser W, Hagberg G, Mader I, et al. Proton MRS of gadolinium-enhancing MS plaques and metabolic changes in normal-appearing white matter. *Magnetic Resonance In Medicine: Official Journal Of The Society Of Magnetic Resonance In Medicine / Society Of Magnetic Resonance In Medicine* 1995;33:811-817.

116. Leary SM, Davie CA, Parker GJ, et al. 1H magnetic resonance spectroscopy of normal appearing white matter in primary progressive multiple sclerosis. *J Neurol* 1999;246:1023-1026.

117. Barreiro CJ, Williams JA, Fitton TP, et al. Noninvasive assessment of brain injury in a canine model of hypothermic circulatory arrest using magnetic resonance spectroscopy. *The Annals Of Thoracic Surgery* 2006;81:1593-1598.

118. Corbett RJ, Purdy PD, Laptook AR, et al. Noninvasive measurement of brain temperature after stroke. *AJNR American Journal Of Neuroradiology* 1999;20:1851-1857.

119. Barker PB, Blackband SJ, Chatham JC, et al. Quantitative proton spectroscopy and histology of a canine brain tumor model. *Magnetic Resonance In*

*Medicine: Official Journal Of The Society Of Magnetic Resonance In Medicine / Society Of Magnetic Resonance In Medicine* 1993;30:458-464.

120. Barker PB, Breiter SN, Soher BJ, et al. Quantitative proton spectroscopy of canine brain: in vivo and in vitro correlations. *Magnetic Resonance In Medicine: Official Journal Of The Society Of Magnetic Resonance In Medicine / Society Of Magnetic Resonance In Medicine* 1994;32:157-163.

121. Lee SH, Kim SY, Woo DC, et al. Differential neurochemical responses of the canine striatum with pentobarbital or ketamine anesthesia: a 3T proton MRS study. *J Vet Med Sci* 2010;72:583-587.

122. Martin-Vaquero P, da Costa RC, Echandi RL, et al. Magnetic resonance spectroscopy of the canine brain at 3.0T and 7.0T. *Res Vet Sci* 2012;93:427-429.

123. Ober CP, Warrington CD, Feeney DA, et al. Optimizing a protocol for (1) H-magnetic resonance spectroscopy of the canine brain at 3T. *Vet Radiol Ultrasound* 2013;54:149-158.

124. Warrington CD, Feeney DA, Ober CP, et al. Relative metabolite concentrations and ratios determined by use of 3-T region-specific proton magnetic resonance spectroscopy of the brain of healthy Beagles. *Am J Vet Res* 2013;74:1291-1303.

125. Ono K, Kitagawa M, Ito D, et al. Regional variations and age-related changes detected with magnetic resonance spectroscopy in the brain of healthy dogs. *Am J Vet Res* 2014;75:179-186.

126. Christiansen P, Henriksen O, Stubgaard M, et al. In vivo Quantification of Brain Metabolites by H-MRS Using Water as an Internal Standard. *Magnetic Resonance Imaging* 1993;11:107-118.

127. van der Toorn A, Dijkhuizen RM, Tulleken CA, et al. Diffusion of metabolites in normal and ischemic rat brain measured by localized 1H MRS. *Magnetic Resonance In Medicine: Official Journal Of The Society Of Magnetic Resonance In Medicine / Society Of Magnetic Resonance In Medicine* 1996;36:914-922.

128. Lei H, Poitry-Yamate C, Preitner F, et al. Neurochemical profile of the mouse hypothalamus using in vivo 1H MRS at 14.1T. *NMR In Biomedicine* 2010;23:578-583.

129. Tamaki N, Yasuda M, Matsumoto S, et al. Cerebral energy metabolism in experimental canine hydrocephalus. *Child's Nervous System: Chns: Official Journal Of The International Society For Pediatric Neurosurgery* 1990;6:172-178.

130. Hattingen E, Pilatus U, Franz K, et al. Evaluation of optimal echo time for 1H-spectroscopic imaging of brain tumors at 3 Tesla. *J Magn Reson Imaging* 2007;26:427-431.